EFFECT OF OPERATING CONDITIONS ON PRODUCT QUALITY IN CONTINUOUS EUTECTIC FREEZE CRYSTALLIZATION

Jemitias Chivavava

Dissertation submitted in fulfilment of the requirements for the degree of Master of Science in Engineering

Department of Chemical Engineering
Faculty of Engineering and Built Environment
University of Cape Town

October, 2013

***Declaration*:** *I know the meaning of plagiarism and declare that all the work in the document, save for that which is properly referenced, is mine*

.....

Acknowledgements

I would like to express my gratitude to the Crystallization and Precipitation Unit for their constant assistance during the course of this project. It has been a pleasure working with such a diverse team full of energy, dedication and brotherhood. A special thank you to my supervisor Professor Alison Lewis for the guidance throughout the course of this work, I really enjoyed the brainstorming exercises that characterised our meetings and seminars.

Deep appreciation goes to Marcos Rodriguez-Pascual for assisting in the design and fabrication of equipment for the experimental set up. Your input into this work was invaluable. To Michael, Brian, Tim, Craig and Umraan thank you so much guys I learnt a great deal from you and I really appreciate your input into this work.

Many thanks to Edward, Derrick and Vuyiswa for your contributions in their various forms. To the rest of the Chemical Engineering Department members, thank you for all the support during my stay here.

Moses thank you for the brainstorming, positive criticisms, encouragement and your assistance with the experimental rig is equally valued. Your encouragement and company even away from laboratory is duly appreciated. Noe thanks for the patience and all the moral and emotional support. Thank you for a job well done! To all my brothers and sisters, I know the frustration and emotions …...!

Summary

The efficiency of gravitational separation in a staged continuous Eutectic Freeze Crystallization process is largely influenced by the quality of solid products exiting the crystallizer. The particle size distribution and shape of the crystalline products affect the efficiency of the washing and filtration steps hence the ultimate purity of the product water and or salts. These characteristics are the net effect of the crystallizer operating conditions such as the level of supersaturation, residence time and magma density. In order to control the mentioned product characteristics, the mechanistic interaction of crystallizer operating conditions and product morphology and size needs to be understood. This work was aimed at investigating the effect of residence time and supersaturation on the product quality in continuous Eutectic Freeze Crystallization and a 2L glass crystallizer equipped with scrapers was employed for the investigations. Image acquisition equipment and image analysis, using MatlabR2011®, were used for particle size measurements and Atomic Absorption Spectroscopy for sodium sulphate concentration determination. The mean particle size of the ice product increased with increasing residence time under isothermal crystallizer conditions. Operating at a lower crystallizer temperature enhanced the mean particle size of the ice product at constant residence time. Increasing the nominal residence time allowed more time for growth and, together with agglomeration, resulted in large particle sizes. Larger sizes obtained at lower operating temperatures were motivated by agglomeration due to high magma density. A mixture of plate-like and elongated disks of ice were observed and no significant change in morphology was observed with both variables in the intervals investigated.

Table of Contents

List of Figures

List of Tables

Nomenclature

a	Activity (kg/kg solvent)
a^*	Equilibrium activity (kg/kg solvent)
A_{het}	Pre-exponential factor for heterogeneous nucleation
A_{hom}	Pre-exponential factor
B	Nucleation rate(#/m^3 .s)
B_{het}	Heterogeneous nucleation rate
b	Ice solids fraction
C	Concentration of the solute
C_p	Coolant specific heat capacity(J/kg^{o}C)
C*	Solubility or equilibrium concentration (kg/kg solvent)
CSD	Crystal size distribution
cv	Coefficient of variation (%)
G	Growth rate (m/s)
i	Relative kinetic constant(-)
k_B	Boltzmann's constant (J/K)
k_d	Mass transfer coefficient (m/s)
k_g	Growth rate constant
kv	Shape factor(-)
k_N	Nucleation constant
L_D	Dominant crystal size(m)
L_{16}	16^{th} percentile (m)
L_{50}	Median or 50^{th} percentile(m)
L_{84}	84^{th} percentile (m)
$\overline{L}_{10}$	Number based average particle size (m)
M_T	Magma density(kg/m^3 of slurry)
n	Population density (#/m^4)
$\dot{m}$	Mass flux density (kg/m^2s)
PSD	Particle size distribution
p	exponent showing dependence of growth rate on size
Q_{in}	Feed flow rate (m^3/s)
Q_{out}	Product flow rate (m^3/s)
Q_{ice}	Heat released by ice crystallization(J/kg)
Q_{feed}	Sensible heat of feed (J/kg)
Q_{loss}	Heat loss to surroundings(J/kg)
Q_{cool}	Heat absorbed by coolant(J/kg)
Q_{salt}	Heat released by salt crystallization(J/kg)

r_c	Critical cluster size (m)
S	Supersaturation ratio(-)
T	Temperature (^oC)
T*	Equilibrium temperature (°C)
ΔG_V	Gibbs free energy of transformation (J/m^3)
V	Active volume of the vessel(m^3)

Greek symbols

σ	Relative supersaturation or standard deviation
μ	Chemical potential (J/kg)
μ^*	Chemical potential at equilibrium (J/kg)
ΔC	Concentration difference (kg/m^3)
υ	Number of ions in solution
ν	Molar volume(m^3/ mol)
γ	Interfacial surface tension(J/m^2)
θ	Contact angle
ΔT	Supercooling/°C
τ	Residence time (s)
ρ_c	Density of crystals(kg/m^3)

1 Introduction

1.1 Background

The mining and manufacturing industries in South Africa produce bulky quantities of hypersaline brines which are continually increasing due to improved water recycling activities (Reddy et al., 2010). Reverse osmosis, evaporative and cooling crystallization processes are conventionally employed for the treatment of such inorganic salt aqueous solutions. These wastewater treatment technologies however do not completely eliminate the pollution problem, utilise more energy in their operations and produce mixtures of salts which still pose a pollution problem.

The residual salt solubility at low temperatures limits salt product yield in cooling crystallization. Reverse osmosis uses relatively lower energy than evaporative crystallization but produces solutions that are more concentrated and suffers from membrane fouling problems (Randall, 2010). Eutectic Freeze Crystallization (EFC) is a separation technique with potential to recover pure salts and water products from these saline brines (Genceli, 2008). The crystallization step of an EFC process requires less energy than the equivalent in an evaporative crystallization process (Stepakoff & Siegelman, 1973; van der Ham, 1999). EFC can be used for separating temperature sensitive materials, reduces the volumes of brine streams and requires cheaper construction materials since it operates at the lower temperatures.

A continuous EFC process can be employed for treatment of large quantities of brines at low costs. The success of a continuous EFC process heavily relies on the efficiency of separation of the crystalline products from each other and the mother liquor. This efficiency of separation is determined by the quality of the crystalline products, which is largely determined by the residence time in the crystallizer and the prevailing supersaturation. These operating conditions influence the kinetic processes of nucleation, growth and agglomeration which are direct determinants of product quality. Vaessen and co-workers (2003) noted that enough residence time is required for crystals to grow and reach sizes essential for gravitational separation in the crystallizer and in downstream processes. An operating supersaturation which promotes growth over the competitive nucleation and agglomeration should be chosen in order to produce solids which allow easy solid-solid-liquid separation.

Research has been done on EFC and continues to be conducted in an effort to develop the technology, so that it can be applied commercially in industry for process and wastewater treatment.

1.2 Aim

Research targeted at developing an EFC process is currently underway at the University of Cape Town with a broader aim of implementing the technology in the South African mining and manufacturing industries for wastewater treatment and recovery of valuable products. The effect of key process conditions on product characteristics in a continuous EFC process was investigated in this work as part of this developmental scheme. Specifically, this contribution focused on the effect of supersaturation and residence time on the crystal size distribution and morphology.

1.3 Project Scope

This work set out to investigate and understand the influence of crystallizer operating conditions on the characteristics of the solids produced in a continuous EFC process. The operating conditions investigated were limited to the nominal residence time, based on the feed flow rate, and operating temperature. Although the quality of crystalline products is described by particle size distribution, morphology and purity, this work focused on the effect of operating conditions on the first two characteristics since these directly influence the efficiency of separation in the downstream stages hence purity of the ultimate product.

Synthetic sodium sulphate aqueous solutions with compositions of between 3.4 and 5 wt% were employed for investigations and residence times between 10 and 45 minutes were investigated. The same mechanical power input per unit volume of slurry, constant stirrer and scraper rotational speeds were employed in all the investigations conducted.

1.4 Plan of Development

This report is divided into four broad sections with Chapter 2 outlining the theory behind crystallization and the fundamentals aspects of this unit operation. A brief description of the operation principle behind eutectic freeze crystallization is also included in this chapter. Chapter 3 reviews Eutectic Freeze Crystallization related work conducted by others, operating conditions and their effect on product quality is then reviewed. Details of the experimental set up and methodology adopted for investigations in this work are presented in

Chapter 4. The obtained results are presented in Chapter 5 together with the discussion and Chapter 6 carries the conclusions and Chapter 7 closes with recommendations.

2 Theory

Crystallization refers to the formation of a dispersed solid phase with an orderly lattice structure from a thermodynamically unstable solution or melt. The separation technique is employed in a wide range of applications in the pharmaceuticals, food, fine chemicals and petrochemical industries to produce highly pure products (Aamir, 2010). Crystallization is driven by the difference in chemical potential between the supersaturated solution and the solid phase or the equilibrium state. This thermodynamic driving force is usually expressed in terms of supersaturation.

2.1 Supersaturation

The absolute supersaturation which is the fundamental driving force for crystallization is expressed as:

$$\frac{\mu-\mu^*}{RT} = v \ln\left(\frac{a}{a^*}\right) \quad 2.1$$

$$\frac{\Delta\mu}{RT} = v \ln\left(\frac{\gamma C}{\gamma^* C^*}\right) \quad 2.2$$

where μ and μ* are the chemical potentials of the supersaturated solution and the solid crystal phase respectively, R is the universal gas constant, T is absolute temperature and a is the activity, c is a measure of concentration, γ is the activity coefficient and v is the number of ions in solution. Activity coefficients are normally assumed constant and the above equation when applied to non-electrolytes is simplified to:

$$\sigma = \frac{C - C^*}{C^*} \quad 2.3$$

Supersaturation is normally expressed in terms of solute concentration in a solution and the solubility or equilibrium concentration of the solute at a given temperature. The latter form of the equation is usually used as a measure of supersaturation in crystallization because concentrations can be measured easily compared to activity. In melt crystallization, supersaturation is expressed as difference between the actual temperature and melting temperature:

$$\Delta T = T^* - T \quad 2.4$$

The same form of equation is sometimes used to express of the level of supersaturation in cooling crystallization operations where solubility is a function of temperature with the solubility temperature replacing the melting temperature.

Figure 2.1 shows two different ways of expressing supersaturation of a moderately soluble solid in terms of operating concentration and temperatures and solubility values.

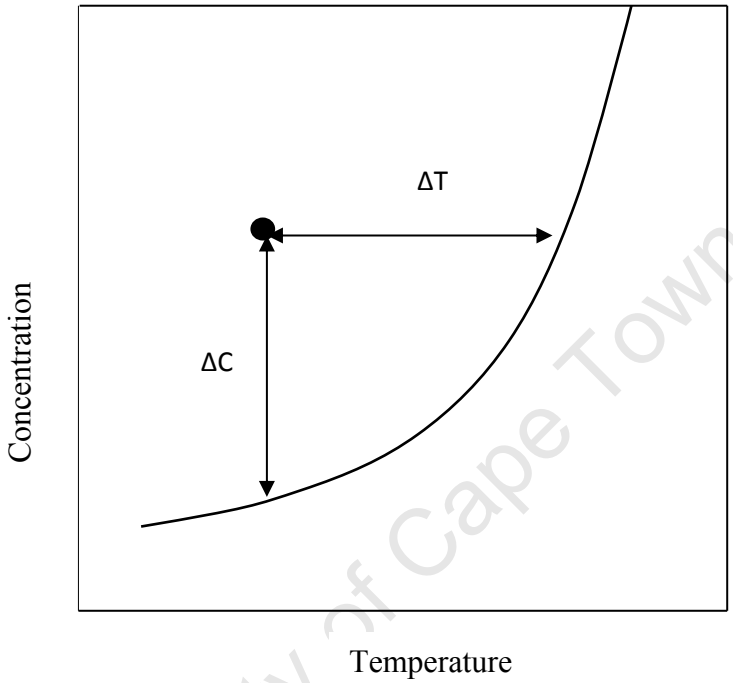

Figure 2.1: Supersaturation of a moderately soluble solute

2.2 Nucleation

This is the first step in the crystallization process and refers to the birth of a highly ordered, stable solid phase from a supersaturated solution, melt or vapour. It occurs through either primary or secondary nucleation mechanisms.

2.2.1 Primary nucleation

Primary nucleation is the initial formation of a solid from a supersaturated solution or melt, which is free of suspended particles of the material to be crystallized and can be subdivided into homogeneous and heterogeneous nucleation (Jones, 2002; Mullin, 2001). The process is termed homogeneous if nuclei form spontaneously from a solids free, highly supersaturated solution (Rawlings et al., 1993). Homogeneous nucleation can be explained using the classical nucleation theory postulated by Volmer and Weber (1926) (as cited by Mullin, 2001) which is based on the Gibbs' concept of a critical size of nucleus. According to this

theory, constituent units of the crystallizing component should form stable clusters of critical size, defined by Equation 2.5, before growing into crystals (Mullin, 2001).

$$r_c = -\frac{2\gamma}{\Delta G_V} \quad 2.5$$

where ΔG_v is the change in Gibbs free energy of transformation per unit volume and γ is the interfacial surface tension. The rate proposed for homogeneous nucleation is shown in Equation 2.6:

$$B_{hom} = A_{hom}\exp\left(-\frac{16\pi\gamma^3\nu^2}{3T^3{k_B}^2(\ln S)^2}\right) \quad 2.6$$

where A_{hom} is the pre-exponential factor, k_B is the Boltzmann constant in J/K, S is the supersaturation ratio and ν is the molecular volume in m^3/mol.

The formation of new particles from a solution or melt facilitated by the presence of foreign insoluble material is termed heterogeneous nucleation (Hattaka, 2010). The free-energy barrier for nuclei formation in the presence of foreign particles is substantially reduced and nucleation occurs at lower supersaturation levels than in homogeneous nucleation (Hattaka, 2010). The heterogeneous nucleation rate is expressed by Equation 2.7 (Markov, 1995; Jones, 2002):

$$B_{het} = A_{het}\exp\left(-\frac{16\pi\gamma^3\upsilon^2 f(\theta)}{3T^3k^2(\ln S)^2}\right) \quad 2.7$$

where $f(\theta)$ is a geometric factor, which varies between 0 and 1, and is defined as shown by Mullin (2001):

$$f(\theta) = \frac{(2+cos\theta)(1-\cos\theta)^2}{4} \quad 2.8$$

In Equation 2.8, θ is the wetting or contact angle between the foreign particle and the crystalline deposit, which varies between 0 and 180 °.

2.2.2 Secondary nucleation

Secondary nucleation refers to the formation of new crystals catalysed by the presence of parent crystals in a supersaturated or supercooled solution (Estrin and Wey, 1973). Less energy is required for secondary nucleation as explained by Jones and Ulrich (2006) and new

crystal formation occurs at much lower supersaturations than in heterogeneous primary nucleation. Secondary nuclei are formed through initial breeding, collision breeding and fluid shear, which removes structured assemblies from the surface of parent crystals. Collision breeding is the most dominant secondary nucleation mechanism in majority of industrial crystallization operations (Jones and Ulrich, 2006; Daudey, 1987).

Secondary nucleation is the dominant nucleation mechanism in continuous crystallization processes (Swenne, 1983) and it is a function of supersaturation, agitation (Hossein & Da-Wen, 2011) and solids content. Its rate is usually expressed as a function of the magma density (M_T), supersaturation (ΔC) and stirring rate (N_s) as summarised in Equation 2.9.

$$B_{sec} = k_N M_T^j N_s^h \Delta C^n \qquad 2.9$$

The exponents j, h and n show the order of dependence of secondary nucleation on suspension density, agitation and supersaturation respectively.

The suspension density affects secondary nucleation through inter-particle collisions and crystals' interaction with the crystallizer's internal mechanical structures and walls. The stirrer speed mainly influences the removal of loosely held assemblies on the stagnant layer surrounding crystals through shear while the level of supersaturation determines the survival of sub-critical clusters into nuclei. The nucleation rate directly influences the crystal size distribution as it controls the nuclei population density hence total surface area available for growth.

2.2.3 Seeding

The introduction of small crystals of the crystallizing solid into a supersaturated solution or melt to initiate nucleation is called seeding. This provides a starting surface area for crystal growth and prevents spontaneous nucleation (Yu, 2007). The provided surface area should be large enough to prevent additional nucleation at the moment crystallization is started to reduce instances of bimodal crystal size distributions. Continuous seeding retards the effective nucleation order and stabilises the system quickly at start up and after a perturbation (Mullin, 1999).

Three critical parameters in seeding policy include seed loading, seeding time and seed size. Jones and Ulrich (2006) indicated that the state of seed material (dry or in suspension), seed surface quality and the point of addition in a crystallizer are also important factors to

consider. Jones and Ulrich (2006) recommend that seeds be small enough and of a quantity that results in high yields and desired product size distribution. A good supersaturation control strategy and seeding procedure can allow a crystallization process with reproducible product quality (number and size).

2.2.4 Growth

Crystal growth is an increase in crystal mass or characteristic dimension driven by non-equilibrium thermodynamic conditions (Myerson and Ginde, 2002; Jones and Ulrich, 2006). Growth rate is a material specific characteristic influenced by supersaturation, hydrodynamic conditions, solution history, and nature of crystal surface, temperature and impurity content of the mother liquor.

Several theories were postulated to describe the crystal growth process, which, according to the diffusion-reaction theory, comprises diffusion and surface integration steps in series as shown in Figure 2.2. Lattice units of the crystallizing solid diffuse from the bulk solution to the solid-liquid interface where they are incorporated into the crystal structure by occupying sites of minimum energy. The growth step is controlled by either solute mass transfer resistance or surface integration kinetics in solution crystallization processes and further influenced by heat transfer resistance in melt crystallization processes. Huige (1972) explained that all the three main processes of heat transfer, mass transfer and in-building of water molecules into the ice crystal lattice influence the growth rate of ice from aqueous solutions.

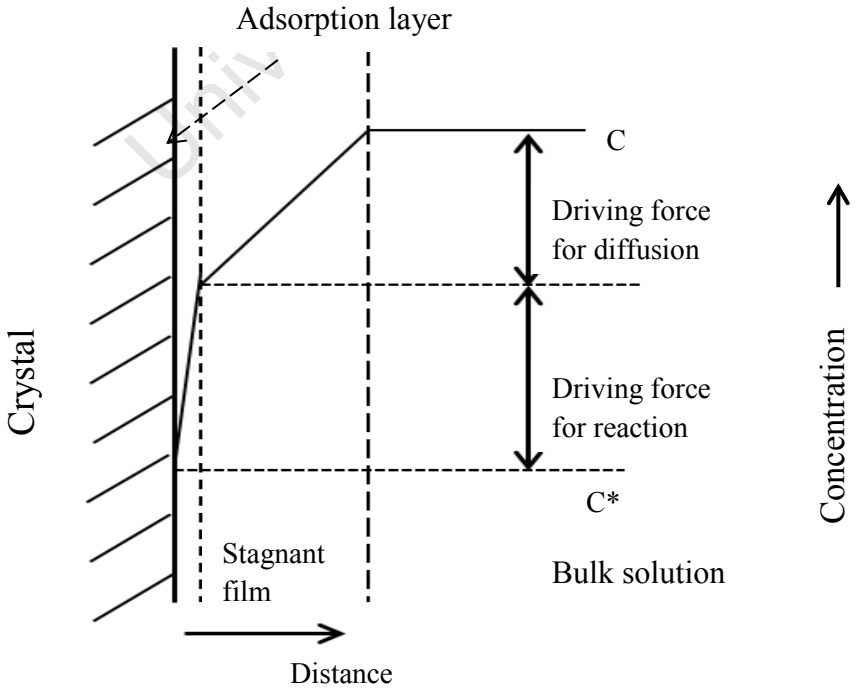

Figure 2.2: Solid-liquid interface for a growing crystal (Adapted from Aamir, 2010)

In a mass transfer controlled crystal growth process, the surface integration reaction is extremely fast and the diffusive-convective transport of growth units from the bulk to the crystal surface can be represented by the Equation 2.10:

$$\dot{m} = k_d(C - C_I) \qquad 2.10$$

where $\dot{m}$ is the mass flux density, C solute bulk concentration and C_I is the interfacial or surface solute concentration.

Mass transport of growth units from the bulk to the crystal surface is very rapid in an integration controlled crystal growth system and the slower surface integration step determines the overall growth rate (Mersmann et al., 2001). Growth rate can be described by the Burton Cabrera and Frank (BCF) model, birth and spread model (BS) and polynuclear mechanism. The screw dislocation (BCF) theory postulates that crystal growth rate has a quadratic and linear relationship with supersaturation at low and high values respectively (Mullin, 2001 and Mersmann et al., 2001).

The rate and mechanism of growth determine the morphology and, together with nucleation rate, the size distribution of the crystallizing solid. The growth rate of geometrically similar crystals is often assumed independent of size and related to supersaturation according to Equation 2.11 (McCabe, 1929) (as cited by Mullin (2001)):

$$G = k_g S^g \qquad 2.11$$

where k_g is a growth rate constant, S is the supersaturation ratio and g is the order of growth. Size-dependent growth and growth rate dispersion models are used to explain the relationship when the above assumptions are violated. Growth rate dispersion occurs when crystals of the same size exhibit different growth rates under identical conditions while in the former it is a function of crystal size, L, as shown in Equation 2.12:

$$G = k_g\, S^g (1 + \gamma L)^p \qquad 2.12$$

Crystal growth rate directly influences the retention time necessary in the crystallizer to reach the required crystal size range (Jones and Ulrich, 2006). Growth rates of crystals can be

estimated from single crystals by measuring the increase in mass or chosen characteristic dimension per unit time or from population density size distribution data analysis.

2.3 Phase diagrams

These are thermodynamic diagrams showing phases present at equilibrium at specific conditions of composition, temperature and pressure. In solid-liquid processes, typical of cooling crystallization, the effect of pressure is insignificant and phase diagrams are usually constructed using temperature and composition as variable parameters. Phase diagrams are useful in determining operating conditions and predicting theoretical quantities of product solids and residual liquid solution after equilibration. Figure 2.3 shows a phase diagram for a binary electrolytic aqueous system, which exhibits eutectic behaviour.

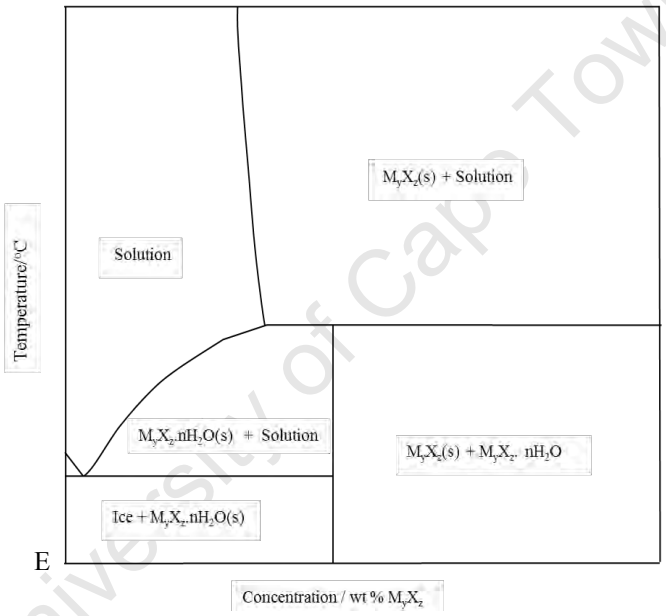

Figure 2.3: A phase diagram of a binary aqueous system

Phase diagrams of multicomponent solutions are more complex than those of binary solutions. The presence of many solutes in a solution can potentially alter solubility and eutectic points. Three-dimensional graphs are usually employed to represent ternary phase diagrams and Figure 2.4 shows a Janecke projection of a typical ternary solution phase diagram, which can be used to decide the operating conditions and estimate the quantities of solids expected to form at chosen operating conditions.

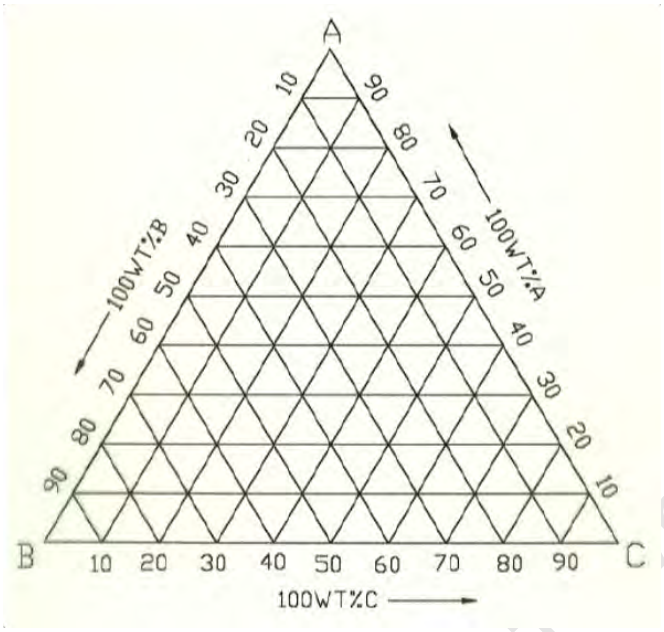

Figure 2.4: A phase diagram for a multi-component ternary system comprising A, B and C (Selvaduray, 2000)

2.3.1 Metastable zone

Metastability is a condition whereby a solution is supersaturated with respect to a given solute or solvent with no solid phase formation reaction occurring. This occurs in a region lying between the solubility or freezing line and the spontaneous nucleation curve or metastable limit. The thickness of this region is termed the metastable zone width. The metastable zone width is a kinetic property dependent upon solution temperature, cooling rate, solution history, impurities content and mixing (Aamir, 2010 and Himawan, 2005). According to Yu and co-workers (2007), only crystal growth and induced nucleation occur in the metastable region for a specified set of conditions and set up. Operating within the metastable zone precludes spontaneous nucleation and allows better control of the crystallization process.

2.4 Eutectic Freeze Crystallization

Eutectic Freeze Crystallization (EFC) is a separation technique capable of splitting aqueous solutions into highly pure ice and salt products by operating at eutectic conditions (van der Ham, 1999). The formed solid phases are separated from each other and the mother liquor by utilizing gravitational and centrifugal forces which exploit large differences in densities

between the phases. Ice crystals with weight less than buoyancy force floats to the top of the crystallizer and heavier salt product crystals sink to the bottom of the crystallizer.

2.4.1 Advantages and disadvantages of EFC

In principle, EFC can achieve the total conversion of process and waste aqueous streams into valuable salts and ice. This makes the method superior to cooling crystallization whose salt recovery is limited by residual solubility at low temperatures (van der Ham, 1999; Seckler, et al., 2002). Van der Ham (1999) suggested that solid solutions formation and inclusions can be excluded through careful control of the growth process to yield highly pure products. EFC is suitable for the recovery of temperature sensitive materials while preserving volatile components (Tahti, 2004).

Cheaper materials of construction are required due to minimal corrosion at low temperatures characteristic of EFC processes (Huige, 1972; Stepakoff and Siegelman, 1973). The EFC process consumes less energy than conventional Evaporative Crystallization (EC) in the treatment of electrolytic aqueous solutions since water latent heat of fusion demand is approximately six times less than that of vaporisation. Van der Ham (1999) reported a 30 and 65% energy requirement reduction upon using EFC in place of the conventional multi-step EC process for separation of sodium nitrate and copper sulphate from aqueous solutions respectively.

EFC becomes economically unviable for aqueous solutions with very low eutectic temperatures since the surface area required for heat transfer is very large. As a new technology EFC, equipment costs are high but these would decrease with time as better designs of the process are developed. The major limitation in EFC is heat exchanger surface fouling which severely reduces the heat transfer coefficient hence heat flux and leads to stagnation of the crystallization process.

2.4.2 Principle of operation

Eutectic Freeze Crystallization achieves separation of process and waste aqueous streams into highly pure solids by operating at eutectic conditions. Van der Ham (1999) noted that both organic and inorganic contaminants can be separated from aqueous streams. A binary phase diagram shown in Figure 2.5 can be used to explain the operation principle of an EFC process.

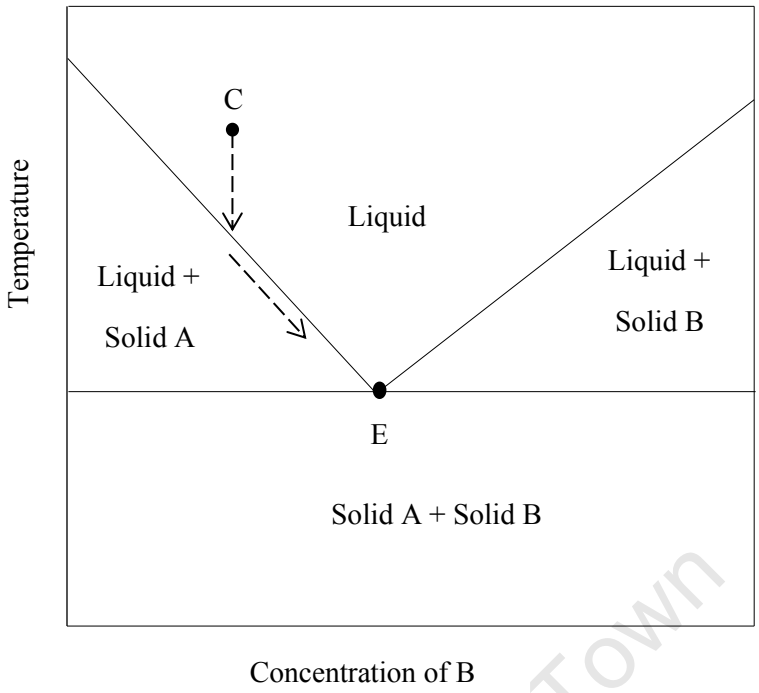

Figure 2.5: Phase diagram of a binary aqueous inorganic system

An undersaturated salt solution of composition C becomes supersaturated with respect to ice if its temperature is slowly lowered to values below its freezing point. Further cooling to the metastable limit initiates spontaneous nucleation followed by growth. The removal of water by ice crystallization concentrates the solution until it reaches the eutectic point (E) where the solution becomes saturated with respect to both components.

Simultaneous crystallization of both ice and salt products occurs if cooling is continued to sub-eutectic temperatures. Dropping the temperature of an undersaturated hyper-eutectic mixture would follow a similar trajectory except that solid B (salt) would form first once the metastable limit is reached. The solution would approach the eutectic point from higher compositions since the removal of B dilutes the solution with both products crystallizing out once the temperature is lowered to sub-eutectic values.

Separation of the formed solid phases from the slurry mixture is accomplished by exploiting differences in density, which allows sinking and floating of salt and ice respectively. This gravity-induced separation between ice and salt crystalline products is achievable within a eutectic crystallizer at adequately low agitator speed (Vaessen et al., 2003). An optimal agitation level necessary to accommodate solids suspension for good mass transfer rates, heat transfer and solid/solid separation requirements should be applied. As explained by Witkamp and co-workers (2001), particle size and shape of the products also influence the efficiency of

gravitational separation in EFC process. In order to achieve gravitational separation in a continuous EFC process larger crystal sizes should be obtained and van der Ham (1999) suggested that spherical sizes of about 100 μm average size would be ideal.

2.5 Heat Transfer in Eutectic Freeze Crystallizers

Supersaturation in EFC processes is created through cooling the solution to sub-eutectic temperatures. Heat released during crystallization and sensible heat is extracted from the crystallizer suspension through direct and indirect cooling methods. Direct cooling employs a refrigerant immiscible with the feed solution and cools the solution by extracting latent heat of vaporisation (Stepakoff et al., 1974). The separation of fine ice crystals produced using this method proved to be difficult and contamination of downstream processing equipment by the coolant made this method of cooling unattractive (Seckler et al., 2002; Himawan, 2005).

Indirect cooling involves heat exchange between the crystallizer suspension and the coolant through a partitioning physical wall. Heat extracted from the suspension is transported away by the circulating refrigerant due to temperature gradient driving force between the two sides of the crystallizer wall. The heat transfer coefficient and total surface area, as noted by Seckler and co-workers (2002), become the critical design parameters for processes based on this method. Vaessen and co-workers (2004) showed that heat transfer from the suspension to a scraped eutectic freeze crystallizer wall is sufficiently described by the penetration theory while the Dittus-Boelter relation modelled transport of the same on the coolant side. Indirect cooling is mainly limited by scale formation on the crystallizer walls which impacts negatively on the crystallization kinetics hence production in eutectic crystallizers (Vaessen et al., 2003; Himawan, 2005).

2.5.1 Heat balance

In continuous cooling crystallization processes the sensible heat of the feed solution and heat of crystallization are both removed during crystallization. In EFC operations heat is released by crystallization of both ice and salt species (van der Ham, 1999) and the heat removal from the eutectic crystallizer can be summarised using the relation in Equation 2.13:

$$Q_{cool} = Q_{feed} + Q_{ice} + Q_{salt} + Q_{loss} \qquad 2.13$$

where Q_{cool} is the heat absorbed by the coolant, Q_{feed} is the sensible heat of the feed, Q_{salt} and Q_{ice} is the heat of crystallization for salt and ice respectively and Q_{loss} is the heat ingress from

the environment. The heat absorbed by the coolant is estimated from the coolant flow rate and temperature change between the inlet and outlet using the relationship shown in Equation 2.14:

$$Q_{cool} = \dot{m} C_p \Delta T' \qquad 2.14$$

where $\dot{m}$ is the coolant mass flow rate, C_p is the coolant specific heat capacity and $\Delta T'$ is the temperature change.

2.5.2 Heat exchange surface fouling

The crystallizer walls functioning as the heat exchange surface experience the lowest temperature within the crystallizer resulting in higher supersaturation levels close to the surface than in the bulk solution in indirectly cooled systems (Rodriguez et al., 2008). This high local supersaturation prevailing on the colder heat exchanger surface prompts excessive nucleation and growth of an ice scale layer on the heat exchanger surface as endorsed by (Himawan, 2005). The heat extraction rate from the bulk solution is subsequently reduced thus adversely affecting the production rates of ice and salt in an EFC process as these directly depend on the magnitude of heat removal rate (Rodriguez, 2009).

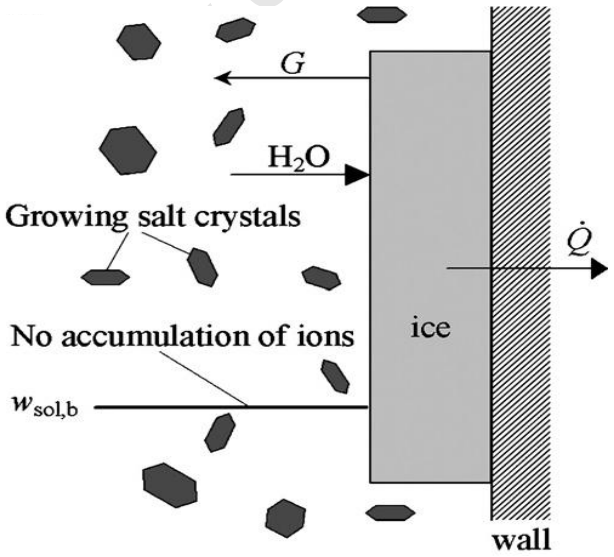

Figure 2.6: Scale formation during EFC (Adapted from Pronk, 2006)

The problem of scale formation in Eutectic Freeze Crystallization stimulated a lot of research focusing on mitigating the challenge through various innovative designs employing mechanical means of cleaning the heat exchanger surfaces (Vaessen, et al., 2003; Himawan,

2005; Genceli, 2008; Rodriguez, 2008). Addition of non-crystallizing components can minimise ice scale formation as shown by Vaessen and co-workers (2003) who reported that nitric acid reduced the incidence of ice scale formation in the EFC of KNO_3. The formation of the ice scale layer on the crystallizer surface can also be minimised by operating at very low temperature driving forces but this results in correspondingly low production rates of ice and salt.

2.6 Continuous Crystallization

Continuous crystallization processes are normally employed for the treatment or synthesis of bulky quantities of materials (Mersmann, 2001) and production of a single product of consistent quality. Batch crystallization is usually employed for synthesis of small volumes of high value specialty chemicals. It is preferred over continuous when the material being processed severely fouls the vessel and there is need to produce a number of products using the same vessel. Although flexible and simple (Rawlings et al., 1993), batch crystallizers are labour intensive and become expensive for large volumes above 10 000 kg/day. Continuous crystallizers allow treatment or processing of quantities above 50 000 kg/day at comparatively lower capital, energy and labour costs.

2.6.1 Residence time

The amount of time spent by a fluid or solid in a vessel or reaction environment is called its residence time. Fluid elements and solids (with a distribution of sizes) spend different times in real reaction vessels, which are best described by residence time distribution functions. However, an average residence time can be used as reasonable estimate of duration in the crystallizer under the assumption of constant suspension volume and adequate mixing. This nominal retention time is estimated as a ratio of the suspension volume to the volumetric feed flow rate as shown in Equation 2.15.

$$\tau = \frac{V}{Q_{in}} \qquad 2.15$$

Alternatively, the average duration in the crystallizer can be approximated as the ratio between the crystallizer solid content and the production rate as summarised in Equation 2.16:

$$\tau = \frac{M_T}{Q_{out}} \qquad 2.16$$

In the above equation, M_T is the mass of crystals in the suspension, τ overall mean residence time and Q_{out} the product withdrawal rate. The value estimated using Equation 2.16 is assumed to closely approach the crystalline product residence time in crystallizers with hydrodynamic conditions similar to those of a mixed suspension, mixed product removal (MSMPR) crystallizer. Han and Shinnar (1968) showed more rigorous ways of estimating residence time but values estimated using Equation 2.15 were considered adequate for investigations in this work.

The time spent by particles in a moderately mixed crystallizer, in conjunction with kinetics of nucleation and growth, determine the ultimate particle size and shape distribution under the constraints of mass conservation requirements. The importance of this relationship in the design and operation of crystallizers prompted several researchers to develop models aimed at predicting the interaction between residence time and mean crystal size. Premised on the assumptions of an ideal MSMPR crystallizer, predictions by Randolph (1965), Mullin (2001) and Jones (2002) all showed that the dominant crystal size, L_D varies with mean residence time according to Equation 2.17:

$$L_D = k\tau^{\frac{i-1}{i+3}} \qquad 2.17$$

Where i is the relative nucleation to growth kinetic order and k is a constant defined by Equation 2.18:

$$k = \left[\frac{3^{i+2}}{2\rho_c k_v k_N}\right]^{\frac{1}{i+3}} \qquad 2.18$$

where ρ_c is the crystal density, k_v is the shape factor and k_N is the nucleation rate constant. The relative kinetic constant, i is the ratio n/g after combining Equations 2.9 and 2.11. Jones (2002) showed that the relationship between the dominant size and residence time can be predicted using graphs in Figure 2.7.

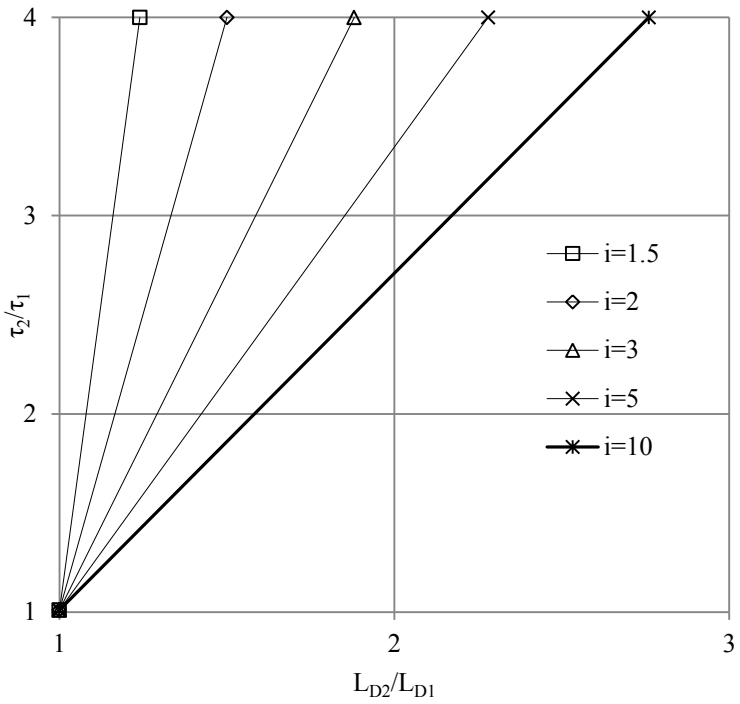

Figure 2.7: Relationship between dominant size and residence time

The overall residence time is an important design and operational parameter that determines the geometric size of the crystallizer as well as the production rate (Fakatselis, 2002). It should be sufficient for product crystals to attain sizes suitable for solid-solid-liquid separation especially in an EFC process.

2.6.2 Suspension density

Suspension or magma density refers to the amount of solids contained in a unit volume of the crystallizer slurry (Mullin, 2001). It is determined by the feed concentration, heat extraction rate and the residence time of the supersaturated solution in the crystallizer. The operating magma density influences crystallization kinetics, through secondary nucleation and providing surface area for growth, productivity as well as suspension rheology or flow properties (Tahti, 2004). In order to prevent product outlet blockages, Vaessen and co-workers (2003) recommend operating crystallizer solid content of less than 40 wt% in EFC processes. Between 5 and 26 wt% ice content and 3 to 13 wt% salt were reported in the top and bottom slurry, respectively, in typical EFC experiments by Genceli (2008) and Rodriguez and co-workers (2008).

2.6.3 Mixing

Mixing ensures a homogeneous temperature and concentration throughout the crystallizer. In suspension crystallization, the stirrer rotational speed should exceed certain threshold in order to just suspend crystals off the crystallizer bottom. Operating at stirrer rotational speed slightly above this minimum allows sufficient mass transfer performance in agitated vessels without excessive crystal attrition (Mullin, 2001). The mixing efficiency determines the spatial uniformity or gradient of solution temperature and concentration in the crystallizer volume hence the variation of local supersaturation.

2.7 Operating Conditions in Continuous EFC

The crystallizer operating conditions largely determine the quality of solid products from a crystallization process. Crystallization processes are usually operated in the metastable region and the common area enclosed by the metastable lines for both ice and salt is the working region where the two solids simultaneously crystallize out of the solution in an EFC process (Vaessen et al., 2003; Himawan, 2005). Himawan and co-workers (2005) showed that the operating point was located at a composition higher than eutectic value for $MgSO_4$-H_2O system while Rodriguez (2008) placed it at eutectic composition for Na_2CO_3-H_2O system.

At a specific composition, the residence time of the feed solution and the heat extraction rate from the crystallizer determine the yield of the crystallizing solids hence the final situation of the operating point. Operating at very long residence times moves the operating point towards the eutectic point as shown by Himawan and co-workers (2005). The feed flow and heat removal rates, as explained by Vaessen and others (2003), should be balanced to maintain a stable solid suspension at sub-eutectic conditions in a continuous EFC process. Figure 2.8 shows the changes in concentration and temperature of an undersaturated feed solution introduced into a crystallizer operating at sub-eutectic conditions.

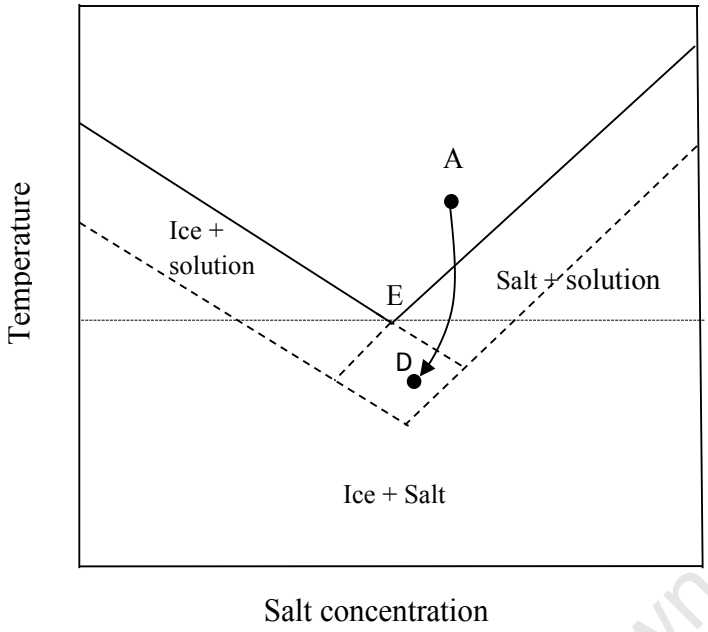

Figure 2.8: Operating region of a continuous EFC process (Himawan, 2005)

At these conditions the feed solution, at temperatures slightly higher than the operating point, mixes and exchanges its sensible heat with the circulating crystallizer contents. The resultant crystallizer concentration and temperature upon mixing the feed and crystallizer slurry are determined by the feed flow rate, composition, enthalpy content and heat removal rate from the crystallizer. Assuming good mixing and sufficient mixing time, the steady state crystallizer solution concentration, as determined by the mixing rule for solutions (Mullin, 2001), lies between the feed concentration and the dilute concentration according to the stream quantities.

The location of the steady state operating point within the common metastable region is determined by the limit of convergence of the transient competitive solute and solvent consumption and addition processes for a specified feed flow rate and concentration assuming non-cyclic crystallizer behaviour. The relative magnitude of ice and salt crystallization kinetics, the feed condition and efficiency of heat removal from the crystallizer decide the ultimate supersaturation level.

The lowest energy state in the presence of the liquid phase, defined by eutectic conditions, gives the thermodynamic boundary of the crystallization process while the location of the actual operating point is governed by kinetic processes. The feed solution acts as a source of fresh supply of both components replenishing those consumed by the rate processes. At steady state, the rate of consumption equals the rate of addition.

2.8 Product Characteristics

The quality of a solid product is usually determined by characteristics such as size, shape and purity. Only size and shape were considered in this work and brief descriptions of these two are given in the following sections.

2.8.1 Crystal size distribution

Products from a crystallization process normally exhibit a distribution of sizes that vary in a definite way over a specific size range. Functions such as normal, log-normal and gamma distributions are used to describe such particle size distributions (PSD). Randolph and Larson (1971) and Mullin (2001) noted that crystal size distributions from crystallizers conform to the gamma-type distribution function. The arithmetic mean, median and dominant size together with the coefficient of variation (cv) are used to characterise crystal size distributions.

The cv which measures the width of the PSD, is estimated from the mean (μ) and standard deviation (σ) of distributions mentioned above using Equation 2.19.

$$\text{cv} = 100\left[\frac{\sigma}{\mu}\right] \tag{2.19}$$

The same coefficient can also be obtained from cumulative weight or number size distribution as shown in Equation 2.20:

$$\text{cv} = 100\left[\frac{L_{84} - L_{16}}{2L_{50}}\right] \tag{2.20}$$

where L_{16}, L_{50} and L_{84} are the 16^{th}, 50^{th} and 84^{th} percentiles from the cumulative undersize curve. The crystal size distribution can be represented in terms of mass, volume, area and number size basis. The size parameter is usually estimated as the circle equivalent diameter estimated from projected area, diameter of a sphere of the same volume and from the mass of the crystal using shape factors and density.

The crystal size distribution (CSD) of products from a batch or continuous crystallization process is a net result of particle generation rate by nucleation, attrition, agglomeration and crystal growth. The interaction between the nucleation and growth processes together with

magma residence time distributions essentially govern CSDs in continuous crystallization processes (Jones, 2002). These product CSDs are of primary importance in EFC as they directly influence separation in the crystallizer and associated downstream processes (Himawan, 2002).

2.8.2 Morphology

The complete characterisation of crystalline products requires specifying the shape and purity to accompany the chosen size characteristic dimension. Crystal shape, often termed morphology or habit, refers to the macroscopic external appearance of crystalline solid particles. This is influenced by the internal spatial arrangement of constituent lattice groups and largely by the relative growth rates of binding external surfaces (direction $\mathbf{a_1}$, $\mathbf{a_2}$, $\mathbf{a_3}$ and **c** in Figure 2.9). The fastest growing crystal faces become smaller and subsequently disappear while the slowest growing faces dominate the final habit of crystals.

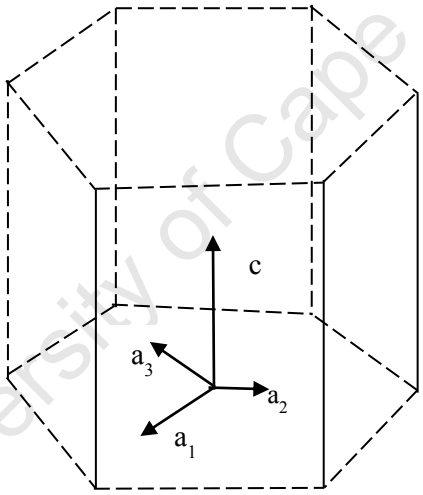

Figure 2.9: Crystal shape development

The crystal habit is determined by both thermodynamic and kinetic factors (Ring,1991), with the former predominating only at very low supersaturations and an equilibrium shape possessing the minimum total surface energy for the crystallized solute volume is expected (Mullin, 2001). Shapes of solids formed at non-equilibrium conditions typical of crystallization processes are primarily governed by kinetics of growth (Mersmann, 2001). Anisotropic growth rates of different crystal flat faces, prompted by dissimilar dependences on supersaturation, temperature, impurity adsorption, surface roughness and crystal size, result in shapes dominated by the slowest growing flat faces. Impurities modify the

morphology of crystals by adsorbing onto the growing crystal faces thereby quickening or slowing down the respective growth rate.

The presence of crystal imperfections in the form of dislocations, twinning and inclusions result in morphological transformations, from flat to pyramidal or conical, stimulated by a spiral growth mechanism which is dominant at very low supersaturation (Ring, 1991; Dirksen and Ring, 1991). Crystal corners grow faster than faces in diffusion controlled growth due to thinner mass transfer boundary layers which offer low resistance ultimately breeding dendrites. A solute concentration gradient instituted by bulk diffusion onto the crystal surface can stimulate faces to change from planar and smooth to spiral growth and step bunching.

Typical crystal shapes include prismatic needle shaped (acicular) and planar plate-like (tabular, platy or flaky). The filterability, flow-ability and compaction behaviour of crystalline products are functionally dependent on the crystal habit (Yu, 2007) and affects the performance of downstream processes as well as handling Yu and co-workers (2007). Shape factors are normally used together with characteristic dimensions to estimate the derived quantities of crystal volumes or surface areas.

2.9 Population Balance Equation

The CSD can be expressed using population or number distribution relating the number or mass of crystals at each size to the mass distribution over the whole size range (Ulrich and Stelzer, 2011). The population balance equation combines the crystal population, the characteristic dimensions and mass balances to describe the distribution of crystal mass in form of different crystal size interval. The population balance model proposed by Randolph and Larson (1971) can be summarised as:

$$\text{Accummulation} = \text{Input} - \text{Output} + \text{net generation} \tag{2.21}$$

$$\frac{\partial(nG)}{\partial L} + \frac{\partial n}{\partial t} + n\frac{\partial V}{\partial t} = B - D - \sum_{k} \frac{n_k Q_k}{V} \tag{2.22}$$

In this equation, G is the linear growth rate (m/s), L crystal size (m), t is time (s), n population density (#/ m^3), V crystallizer active volume (m^3), B birth function and D death

function. The equation is simplified as shown in Equation 2.23, provided the feed contains no suspended solids and the McCabe's ΔL law of size independent growth is assumed.

$$\frac{\partial n}{\partial t} + \frac{\mathrm{G}\,\partial \mathrm{n}}{\partial \mathrm{L}} + \frac{\mathrm{n}}{\tau} = 0 \qquad 2.23$$

where τ is the mean particle residence time in seconds. The population balance equation for a mixed suspension mixed product removal (MSMPR) crystallizer operating at steady state is simplified to Equation 2.24:

$$n = n_o exp \frac{L}{G\tau} \qquad 2.24$$

2.10 Measurement Techniques

The crystal size distribution can be determined by a number of measurement techniques. In the Coulter Counter or zone sensing method, particles are suspended in an electrolyte and drawn through a small orifice containing an electrode on either side. Based on the principle that voltage and pulse frequency are directly proportional to particle volume and number respectively, the CSD is measured on a volume and number basis.

Sieving measures particle sizes between 10 and 5500 μm by using a wide range of sieve sizes. Although simple, portable, inexpensive and widely used, sieving is not suitable for online measurement because it is time consuming and has poor reproducibility (Aamir, 2010). Laser diffraction is based on the principle that particles passing through a laser beam scatter light at an angle directly related to their size with large particles scattering high intensity light at narrow angles and small particles scattering at wide angles but very low intensity. The technique uses Fraunhofer diffraction and Mie scattering theories to obtain CSD from the light intensity distribution and assumes that particles are spherical in shape and suspensions are dilute.

2.10.1 Image analysis

Images of particles are captured using equipment such as transmission electron microscope (TEM), scanning electron microscope (SEM), light microscope, magnetic resonance imaging and video digital cameras. The acquired images are analysed to extract quantitative information like crystal size distribution and morphology of constituent objects of interest. The object characteristic dimensions or attributes are determined after the images have been processed. Image analysis can be directly employed, non-intrusively, for both on-line and off-line particle size and shape measurement (Aamir, 2010 and Yu et al., 2007). The technique is also useful in the classification of crystals based on polymorphic and morphological forms.

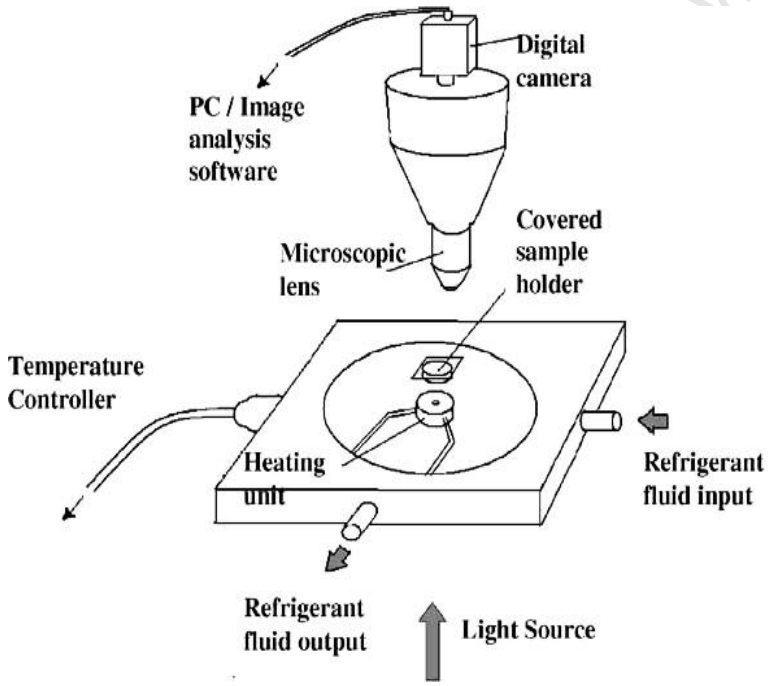

Figure 2.10: Image acquisition using a digital imaging set up (Arellano et al., 2004)

The crystal size distribution is obtained from the projected area in terms of crystal population against perimeter, equivalent diameter and axis length. Circularity, elongation and eccentricity are quantitative characteristic shape/habit indicators obtainable from 2D images. Tahti (2004) stated that image analysis, though tedious, is a truly reliable method for determination of size and shape of crystals.

3 Literature Review

A brief history of the development of EFC is reviewed in the first section of this chapter before previous work related to the effect of operating conditions on product quality is looked at. The last section summarises the problem statement, hypothesis and objectives.

3.1.1 Continuous Eutectic Freeze Crystallization

A continuous EFC process based on the Crystalex process was developed in the 1970s by Stepakoff and Siegelman (1973). They conducted experiments to test the technical feasibility of a continuous EFC process on a 10-15 wt% aqueous KCl solution. A stirred tank crystallizer was employed for the crystallization step and a hydrocyclone used for splitting the resultant slurry into an ice rich overflow and solid salt containing underflow. Direct contact evaporative cooling, using an inert and immiscible refrigerant, provided the necessary cooling requirements.

Using similar equipment and cooling method, Swenne (1983) applied EFC in the production of NaCl and proved its technical feasibility although no industrial application of the process was realised. Van der Ham and co-workers (1999) developed an indirect cooling based 15 L EFC crystallizer for separation of $CuSO_4$ and other industrial inorganic salts from aqueous solutions. The prototype hybrid crystallizer allowed simultaneous crystallization and solid-solid separation in a single vessel while preventing coolant contamination. Circular horizontal disks supplied with a refrigerant provided the necessary cooling hence the name Cooled Disc Column Crystallizer (CDCC). The CDCC disks had orifices on the edges for easy upward and downward transport of crystals. However, the movement of ice and salt through orifices was difficult, hindering effective separation (Himawan, 2005).

Vaessen and co-workers (2003) developed and constructed prototypes of 100L CDCC and 115L Scrapped Cooled Wall Crystallizer (SCWC) for eutectic crystallization of ternary KNO_3-HNO_3 aqueous solutions. The SCWC incorporated an extended cooling surface in form of a cylindrical inner jacket to increase the heat transfer surface area and had conical structures fitted on both ends for efficient collection of both products. Both designs had provisions for vertical movement of both ice and salt crystals in the crystallizer to allow separation through floating and settling of the two phases respectively. However, the SCWC geometry provided a larger separation area compared to the CDCC whose poor

settling-floating exchange between the disk orifices restricted gravitational separation (Vaessen et al., 2003).

In his simulation studies, Himawan (2005) applied EFC technology to recover magnesium sulphate and ice from a flue gas desulphurization plant effluent. The author developed a framework for estimation of crystallization kinetics in an EFC process using the population balance model and investigated the effect of coolant temperature and residence time on CSD. Genceli and others (2005) designed and tested a complete pilot scale CDCC based continuous EFC process for easy integration into industrial plants. The process was designed to produce 130 tonnes/year $MgSO_4.7H_2O$ from an industrial an aqueous $MgSO_4$ solution and the mobile skid included belt filters and washing columns for further separation of products from the mother liquor.

In their work, Genceli and co-workers (2008) demonstrated two possible configurations for continuous EFC processes. One of their proposed processes employs a hybrid crystallizer-separator vessel while the other configuration includes crystallization and separation as two sequential stages. The latter configuration is preferable when solid-solid separation in the crystallizer alone is not satisfactory. Rodriguez (2009) designed and applied an improved version of the eutectic SCWC to recover sodium carbonate and ice from a soda contaminated incinerator liquid effluent exiting an AVR industry.

3.1.2 Effect of residence time on crystal size

The relative kinetic rate between nucleation and growth, at specific supersaturation conditions and suspension density, directly governs the influence of residence time on the product crystal size distribution (Tahti, 2004). While the relationship in Equation 2.17 provides insight into the effect of residence time on the average crystal size, different results regarding this relationship were reported by various workers in practical settings even on the same system.

Margolis and co-workers (1971) investigated the effect of residence time on the crystal size of ice crystallizing out of a 6 wt% sodium chloride aqueous solution in a directly cooled continuous crystallizer. The authors concluded that changing feed flowrate had no noticeable effect on ice crystal size distribution. Two different feed flow rates corresponding to overall residence times of 6.5 and 13 minutes were investigated in this work. While the results established a reasonable relationship between the average size and residence time similar to

that reported for phenol by Verdoes and co-workers (1997), investigations over a wider spectrum of feed flow rates could have corroborated these findings. The investigated range of flow rate was possibly insufficient to notice any significant shift in the CSD. It is possible that due to faster kinetics of ice, the growth rate after 6 mins had actually slowed down hence no significant change realised at 13 minutes holding time.

Investigations by Huige (1972) showed that the average equivalent diameter of ice crystallizing from 10 to 42 wt% dextrose aqueous solutions depended less linearly on the mean crystal residence time. Varying the crystal residence time between 6 and 70 minutes at supercoolings below 0.05 ^{o}C, he showed that the experimental average equivalent diameter (100-250 μm) could be correlated to the mean residence time according to the power law as shown in Equation 3.1.

$$d_e = 2.87 \times 10^{-3} \tau^n \qquad 3.1$$

where d_e is the equivalent diameter and n is the exponent varying between 0.22-0.23. This observation could be attributed to increased mass transfer resistance, due to organic dextrose molecules, which slowed the diffusion step of the growth process. The power law relationship between the average crystal size and holding time was also reported by Swenne (1983) in an EFC process. The author observed an increase in the average crystal size of both $NaCl.2H_2O$ and ice with a decreasing feed flow rate in a directly cooled continuous stirred crystallizer. The obtained relationship however, included solids concentration (b) as summarised in Equation 3.2:

$$\overline{L}_{10} = k b^c \tau^n \qquad 3.2$$

Crystal sizes were obtained from images acquired, from a slurry stream flowing through a discharge pipe, using a light microscope. The investigations were conducted in an 8.5 L crystallizer for residence times between 5 and 42 minutes resulting in mean crystal sizes of 59 to 140 μm for salt and 62 to 170 μm for ice.

In his simulation study, using $MgSO_4$-H_2O system in a pilot scale 100 L SCWC eutectic crystallizer, Himawan (2005) observed an increase in average crystal size of both products with residence time between 1.2 and 1.8 hours at a coolant temperature of -7.2 ^{o}C while no change was observed at -9.2 ^{o}C. The independence of average crystal size from residence time was attributed to secondary nucleation on the crystallizer wall which generated copious

quantities of nuclei at the expense of growth. Size measurements were conducted offline and non-isokinetic sampling due to product classification; and product modifications as a result of handling (Vaessen et al., 2003) possibly influenced the findings especially given that the change observed at -7.2 ^{o}C was not very significant.

However, Russell and co-workers (1999) who reported a decrease in the mean ice crystal size with increasing product throughput in an ice cream manufacturing freezer noted that wall conditions did not determine the steady state size distribution. In this work, investigations separately conducted at constant coolant and draw temperatures yielded similar results. They clearly stated that residence time determined the crystal size. In their research, Drewett and Hartel (2007) observed that residence time had the most pronounced effect on the mean ice crystal size. Their investigations also revealed that the draw temperature and the dasher speed impacted on the mean ice crystal size but to a lesser extent.

Employing an in-situ Focused Beam Reflectance Measurement (FBRM) to measure the crystal chord length, Arellano and co-workers (2012) observed that residence time had an insignificant effect on product crystal size. While the results of these investigations are important guidelines regarding the relationship between residence time and average crystal size, investigated sizes ranged between 10 and 60 μm. This size range would create separation difficulties in EFC (Stocking & King, 1976; Himawan, 2005) and extrapolating the observed effects to large sizes would introduce errors especially considering that some researchers reported size dependent growth of ice crystals (Margolis et al., 1971; Shirai et al., 1986). Extending the investigations to sizes larger than 50 μm would yield more useful results for EFC operations, in which mean sizes of 100 to 200 μm and 50 to 120 μm were reported for ice and salts respectively (Rodriguez et al., 2008; Genceli, 2008).

Verdoes and co-workers (1997) reported an increase in the average crystal size of caprolactam with residence time in a 3L laboratory scale continuous crystallizer. In their investigations, Nienoord and Verdoes (1999) revealed that the average crystal size of potassium nitrate crystallizing out of an acidic aqueous solution increased upon doubling residence time from 30 to 60 minutes. A similar conclusion was reached by Vaessen and co-workers (2003) when they applied EFC to a potassium nitrate water system. In their investigations a significant change in the average crystal size with residence time, scraping rate and subcooling was observed. The overall residence time was changed between 1 and 2.5 hours in their investigations.

3.1.3 Effect of residence time on crystal morphology

The length of stay in the crystallizer also influences the morphology of crystals. Different crystal shapes result from combination of growth and secondary kinetic processes of attrition, breakage and agglomeration. The residence period in a crystallizer determines the extent of growth and the final shape assumed before withdrawal from the vessel. Sufficiently long durations allow the full growth process leading to the disappearance of faster growing faces and crystal shapes bounded by slowest growing faces. Mersmann (2001) indicated that growth kinetics and lattice structure determined the morphology of crystals of size less than 100 μm.

According to Mersmann (2001) collision mechanisms and fluid shear stresses largely determine the habit of particles bigger than 500 μm. Such particles potentially form if crystal residence in the crystallizer environment is prolonged at low supersaturation. The attrition and breakage induced by the crystal-crystal and crystal-impeller collisions modify the morphology of crystals by abrasion and fracture along dislocations. Crystals exposed to attrition are characterised by rounded shapes bereft of sharp edges.

The change in morphology with residence time is system specific with material properties of the crystals determining the extent of secondary kinetic processes. The susceptibility of crystals to attrition and breakage is a function of fracture resistance and brittleness of the crystallizing solid. Nienoord and Verdoes (1999) showed that KNO_3 crystals became more regular and disk shaped with increasing residence time. KNO_3 was reported to be attrition prone giving round crystals in contrast to attrition resistant KCl whose crystals showed sharp edges (Mersmann, 2001).

The growth on damaged crystal faces is enhanced prompting a change in the relative growth rate of faces consequently altering the crystal morphology during growth time in the crystallizer. The morphology of ice crystals and $MgSO_4.11H_2O$ did not change significantly when residence time changed between 1.1 and 3 hours (Genceli, 2008).

3.1.4 Effect of supersaturation on crystal morphology

The prevailing supersaturation, impurity content and hydrodynamic conditions influence the growth process of the crystallizing solid phase hence the ultimate product shape. Ice, the common crystallizing solid in EFC of aqueous solutions, exhibits a multiplicity of morphologies if grown from pure water and aqueous solutions at different growth conditions as noted by Petzgold and Aguilera (2009).

Several studies in freeze based desalination and food processing have revealed that spherical ice crystals form at very low supersaturations and growth rates while thin disks are produced at relatively high growth rates (Kiani & Sun, 2011; Harriot, 1967; Huige, 1972). Harriot (1967) and Huige (1972) noted that hexagonal, plate-like crystals are expected to form when ice crystallize out of still, supercooled aqueous solutions under atmospheric pressure. Harriot (1967) and Arellano et al., (2012) further specified that operating at supercoolings above 0.1 ^{o}C in salt aqueous solutions increases chances of dendritic growth.

An investigation conducted by Margolis and others (1971) showed that circular and hexagonal disks of ice crystals formed at supercoolings between 0.017 and 0.031 ^{o}C during freeze crystallization from a 6 wt% NaCl aqueous solution. The formation of disks was attributed to inherently faster growth kinetics of the prism faces relative to that normal to the basal plane. In his work, in which bulk solution supercooling was less than 0.05^{o}C, Huige (1972) showed that a mixture of nearly spherical and flat disk ice crystals formed from dextrose solutions of concentration less than 4 wt%. In these investigations the shape was observed using photography and disks height diameter ratio of 0.26, area shape factor of 9.56 and volume shape factor of 1.64 were reported.

Stepakoff and co-workers (1974) observed that ice product with a platelet structure formed in a directly cooled continuous EFC process operating at driving forces between 4 and 7 ^{o}F (2.2 and 3.9 ^{o}C, IUPAC). This is similar to observations by Swenne (1983) who reported round, plate shaped ice crystals at supercoolings of about 0.1^{o}C (Figure 3.1). Cubical KCl crystals were reported by the former and nearly spherical sodium chloride dihydrate crystals by the latter. In his work, Swenne (1983) observed that crystal morphology was independent of operating conditions and crystal size at investigated supercoolings. The crystal morphology was viewed using microscopes and this involved extracting slurries from the crystallizers hence the possibility of destruction of corners and edges induced by abrasion against pipe walls as the slurry flowed through the pipe.

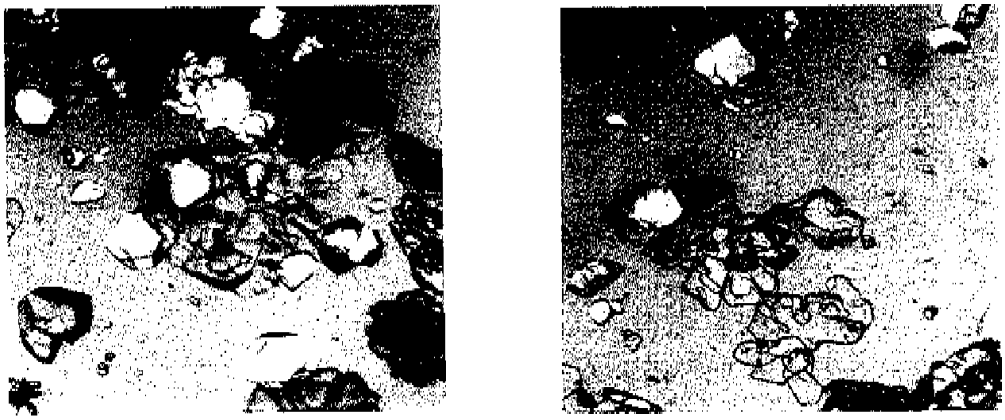

Figure 3.1: Micrographs showing sodium chloride and ice crystals (Swenne, 1983)

An investigation by van der Ham (1999) revealed that round shaped ice crystals formed from a $CuSO_4$ aqueous solution during EFC experiments at operating supercoolings between 0.1 and 0.2 ^oC. In a separate EFC application, Vaessen and co-workers (2003) observed that flat, circular disk-shaped ice crystals and well-faceted potassium nitrate crystallized out of a ternary KNO_3-HNO_3 aqueous solution at a supercooling of about 0.2 ^oC. The supercooling in these two studies shows that ice with disk morphology can potentially crystallize out at higher values than those mentioned by early workers who proposed that chances of dendritic ice formation increases above a supercooling of 0.1 ^oC (Harriot, 1967).

Genceli (2008) observed circular shaped ice and prismatic $MgSO_4.11H_2O$ products crystallized at eutectic conditions in a CDCC when coolant temperature was varied between -7.6 and -11.7^oC. These findings suggest the independence of ice morphology from the influence of the second crystallizing component.

3.1.5 Effect of supersaturation on CSD

The level of supersaturation in a crystallization process influences the CSD of the produced solids through interaction between particle rate processes of growth and nucleation which are driven by this thermodynamic force (Stocking & King, 1976; Helt & Larson, 1977). Nucleation has a stronger dependency on supersaturation than growth and predominantly regulates the crystal size distribution (Garside, 1985). A large nuclei population is formed at high supersaturation levels and the average crystal size becomes very small while growth kinetics is expected to dominate at low supersaturation values. In his studies, Huige (1972) observed that the mean crystal size of ice crystallizing out of an aqueous sucrose solution depended on supercooling according to the power law with an exponent of 0.75. Kane and co-workers (1975) postulated that the average size of ice crystallizing out of a 5.3 wt % salt

solution should vary proportionally with supercooling raised to power -0.75. According to Russell and co-workers (1999), high supercooling generates a lot of ice nuclei population and results in smaller particle sizes.

Himawan (2005) observed an increase in mass based average crystal ice and $MgSO_4.11H_2O$ upon reducing the supercooling level by adjusting coolant temperature from -9.2 to -7.2 ^oC at a constant residence time of 1.8 hours. This phenomenon was attributed to decreasing contribution of secondary nucleation on the crystallizer wall at high coolant temperatures. However this inconsistent with findings by Russell and co-workers (1999) who observed insignificant influence of freezer wall effects on steady state product ice size in ice cream manufacturing. Drewett and Hartel (2007) realised a decrease in the average crystal product size upon increasing the supersaturation level and this same conclusion was reached by Alvarez and Myerson (2010) who attributed this to higher nucleation rates.

Mersmann (2001) and Stocking and King (1976) noted that the effect of supersaturation on CSD is unpredictable due to the uncertainty in the dependence of the nucleation rate on supersaturation especially in agitated suspension crystallizers. The rate of secondary nucleation is dominant in suspension crystallization systems and its dependence on other factors like magma density and stirring rate makes its dependence on supersaturation less predictable a priori. While the relationship between supersaturation and crystal size in systems with a single crystallizing component is well researched on, the simultaneous crystallization of components adds to the already complicated relationship between the two variables.

3.2 Research Motivation

The separation of both ice and salt products from the residual mother liquor in an EFC process functionally depends on their densities, crystal size distributions and morphology. These product properties are determined by the operating conditions of the crystallization step in a multi-stage continuous EFC process and ultimately affect the performance of further separation steps (Stepakoff et al., 1974).

While the heat flux from the crystallizer determines the quantities of ice and salts produced, the quality of the crystallized solid fraction (particle size and shape distribution) determines the efficiency of the gravitational separation hence purity of the final products (Witkamp et

al., 2001). The length of time spent by crystals in a crystallizer and the operating supersaturation directly affects the particle size distribution and morphology of the products through the kinetic processes of nucleation and growth. The operating driving force influences the relative rates between nucleation and growth while the nominal crystallizer retention time determines the extent of growth of the formed nuclei.

An understanding of mechanisms through which operating conditions affect the quality of products is necessary for the development and design of crystallizers capable of producing crystals with specific characteristics. This is important in a staged continuous EFC process where ice and salt particles of a quality suitable for gravitational separation, washing and filtration should be produced. Better control of product particle size distribution and shape requires knowledge of the rates of nucleation and growth.

The splitting of aqueous solutions through simultaneous crystallization of both constituents creates interdependence between the respective crystallization kinetics of the individual components. This complex coupling of components crystallization events makes prediction of the kinetics more involving and less obvious since one component's crystallization behaviour is influenced by that of other components. The extent of the inter-kinetic 'wars' in eutectic systems could be determined by measuring the response of the solid product characteristics to changes in operating conditions.

3.2.1 Aim and Hypotheses

The broader aim of this study was to investigate the effect of operating conditions, of the crystallization step, on the nature of the resultant solid product and it was hypothesized that:

1. Increasing the slurry nominal residence time in an isothermal continuous Eutectic Freeze Crystallizer enhances the average size of both products and widens the particle size distribution.
2. Increasing supersaturation in a continuous EFC process increases the percentage of dendritic ice crystals and increases the width of the particle size distribution.

3.2.2 Key questions

1. How does the supersaturation of both solute and solvent components vary with residence time in an isothermal, continuous EFC process as the two simultaneously crystallize out of solution?

2. How does increasing supersaturation at constant residence time change the ice product average particle size distribution and cv?
3. Which primary kinetic process is influenced by the supersaturation induced by competitive component crystallization?
4. How is the relative kinetic order between nucleation and growth of both products influenced by the mutual supersaturation creation?

3.2.3 Objectives

The main objectives of this work were to:

1. Investigate the impact of changing the operating temperature on crystal size and morphology of products in a continuous EFC process.
2. Investigate the effect of changing residence time on the mean particle size and width of the size distribution of solid products in an isothermal continuous EFC process.

4 Methodology

This section details the equipment employed and experimental procedures adopted in the investigations conducted in this work.

4.1 Experimental design

Sodium sulphate aqueous solutions with compositions between 3.79 and 5 wt% were prepared using analytical grade sodium sulphate and ultrapure water. Three residence times of 20, 30 and 45 minutes were investigated using a 3.79 wt% sodium sulphate feed solution at constant suspension temperature. Heat removal limitations precluded the investigation of residence times shorter than 20 minutes and unreasonably low product withdrawal rates at residence times longer than 45 minutes fixed the longest time investigated for 3.79 wt% feed solution. Operating supercoolings were varied between 0.01 and 0.05 ^{o}C at a constant mean residence time of 30 minutes for 3.79 wt% feed solution.

Preliminary experiments were dedicated to producing sodium sulphate decahydrate as the only product. Feed based nominal holding times of 10, 20 and 30 minutes were investigated using the 5 wt% feed solution. All experiments were conducted in a cooled 2L jacketed glass crystallizer equipped with a mechanism to minimise scale formation as detailed below.

4.1.1 Na_2SO_4-H_2O system

Sodium sulphate is one of the major components in brines generated in South African mining operations and this motivated the use of an aqueous solution of this salt in this study. Sodium sulphate forms a eutectic composition in an aqueous solution between 3.79 and 4.19 wt% and an approximate temperature of -1.2 ^{o}C.

Thernadite (Na_2SO_4) and mirabilite ($Na_2SO_4.10H_2O$) are the two stable phases of sodium sulphate at room temperature and heptahydrate is the metastable form which is normally produced at very low temperatures. Thernadite crystallizes out of an aqueous sodium sulphate solution above the transition temperature of 32.7 ^{o}C while mirabilite preferentially forms at temperatures below this value. Anhydrous sodium sulphate shows an inverse solubility temperature relationship (Treptow, 1993).

4.1.2 Experimental set up

The experimental set-up employed for all experiments conducted in this work is illustrated in Figure 4.1. A 10L glass vessel (T01) equipped with a magnetic stirrer was used as a storage

tank for the feed solution. The magnetic stirrer ensured a homogeneous solution concentration in the storage tank and re-dissolved product salt crystals before the solution was passed to a pre-cooler (PC). The pre-cooler, which was a jacketed glass vessel supplied with Kryo 40 coolant from a Lauda RK 8KP thermostatic unit (H01), reduced the crystallizer cooling duty through removal of the major portion of the feed sensible heat prior to feeding into the crystallizer (C01). This allowed the crystallizer to operate at low temperature driving forces between the coolant and the solution (Mullin, 2001), thus minimising chances of scale formation on the walls. The vessel was constantly agitated using a pitched blade impeller connected to a variable speed IKA overhead stirrer to ensure homogeneous feed solution temperature and concentration, and was insulated to minimise heat ingress from the surroundings.

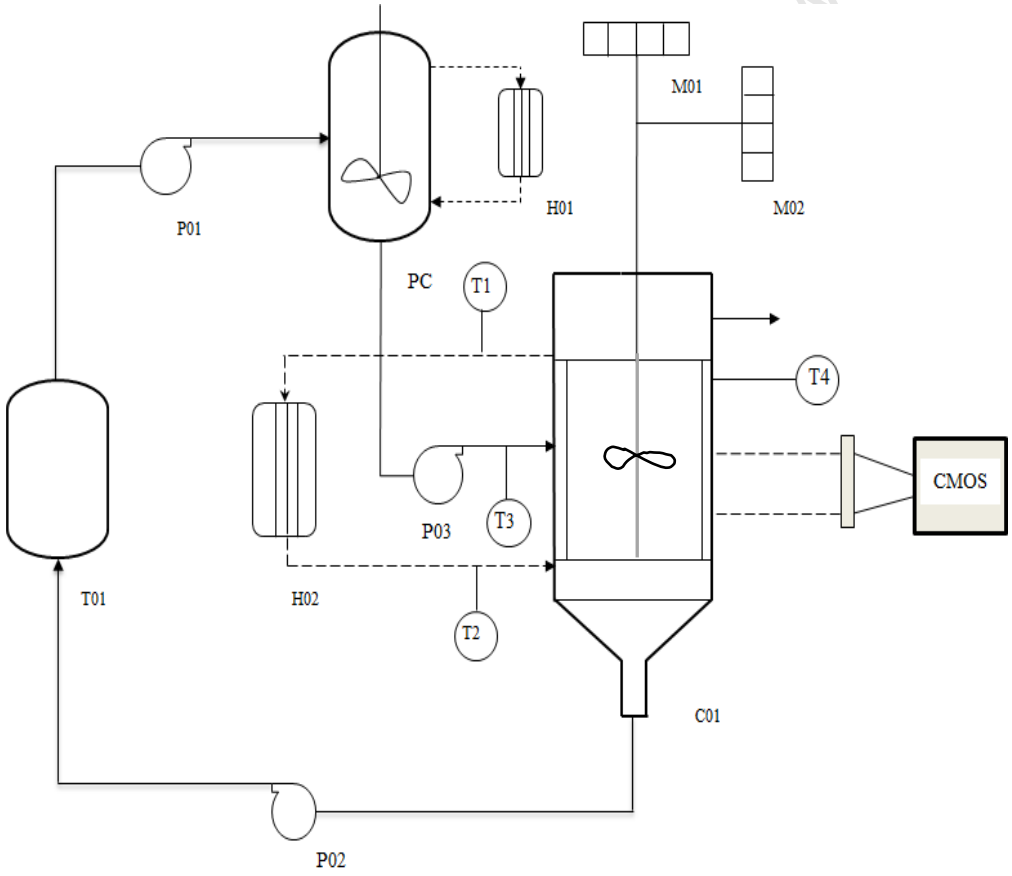

Figure 4.1: Experimental set-up

A glass vessel consisting of three distinct compartments was employed as a hybrid crystallizer-separator. The middle jacketed section, which was cooled by continuous circulation of Kry40 liquid from a Grant GR 150 cooling unit (H02), performed the

crystallizer duty. This was equipped with high density polyethylene (HDPE) scrapers to minimise ice scale formation on the crystallizer walls. Constantly pressed against the crystallizer walls by springs, the scrapers were fastened onto a structural frame which was attached to an outer shaft coupled to a horizontal, variable speed Bonfiglioli motor (M02).

A six blade Rushton turbine stirrer connected to a vertical variable speed Bonfiglioli motor (M01) was employed for agitation and rotated in a direction opposite that of scrapers. The lower compartment of the crystallizer consisted of a cylindrical section affixed with a conical section for efficient collection of salt crystals and channelling towards the outlet spout. The outlet was connected to a peristaltic Watson Marlow pump which recycled the salt product slurry to the storage tank.

The top separation section allowed ice separation and entrained salt disengagement and had an internal cone attached to the shaft in order to break the accumulation of ice induced by centrifugal forces created by the circulating crystallizer contents. A port fitted at 10 mm from the top of the vessel was provided for ice product slurry withdrawal through an overflow mechanism.

4.2 Measurement techniques

4.2.1 Temperature

Platinum resistance thermometers (Pt100) of ±0.01 ^{o}C accuracy level were used to measure temperatures of the feed solution, crystallizer suspension as well as coolant inlet and outlet values. These were connected to an F252 AC precision bridge and a 16-multichannel SB500 expansion switchbox which communicated with a computer via Ulog software which recorded temperature at 5 seconds interval.

4.2.2 Concentration

A syringe fitted with a 0.2 μm filter paper was employed for drawing samples of the residual mother liquor from the crystallizer. Atomic Absorption Spectroscopy (AAS) was then used for sodium ion concentration measurement. The residual mother liquor solute concentration and bulk suspension operating temperature were used to estimate the operating supersaturation.

4.2.3 Residence time

The residence time was estimated from the crystallizer volume and feed solution flow rate using Equation 2.15.

4.2.4 Crystal size and morphology

A transparent coolant was used to allow image acquisition from inside the crystallizer. A high speed GmbH Mikrotron (MC1363) Complementary Metal-Oxide Semiconductor (CMOS) camera, connected to a frame grabber, was used as a sensor and MotionBLITZDirector® software used for image acquisition. A Micro Nikkor 105 mm zooming lens was used to magnify crystals to allow capturing of crystals of at least 30 μm. An optical fibre coupled to a white light source was employed for illumination. An optical imaging window was mounted on the outer wall of the crystallizer to correct wall convexity effects on the light. Image processing and analysis using Matlab R2011® allowed extraction of particle size distribution and morphology information (Brown & Xiong-Wei, 2011).

4.2.5 Image analysis

Crystal images, captured using the mentioned digital camera, were loaded into Matlab R2011b® for processing. These raw images were converted from true colour (red, green, blue (RGB)), to eight bit grayscale intensity images by eliminating hue and saturation values while maintaining luminance.

Figure 4.2: (a) Original image in rgb format (b) Grayscale image after rgb to grayscale conversion

The image background was subtracted from the original image to produce a new image with a homogeneous background. After background subtraction, segmentation followed. This involved partitioning image components into distinct regions of homogeneous luminance

(Starck and Murtagh, 2002). Spatial filtering to remove noise from the images was accomplished using the Gaussian filter.

After the objects were identified, a luminance based thresholding was executed to classify image components into background and foreground objects. Objects with luminance higher than the threshold value were mapped to white luminance display and those with intensity less than this value were regarded as part of the background. Edge detection, which involved identification of boundaries between objects and background of an image, was employed for effective segmentation of some images. After transformation into a binary image (black and white), small holes inside objects were filled in and integrated as part of foreground objects. The crystal size distribution and shape information of the objects in the image was the extracted. The frequency of clusters having projected areas within intervals defined by bin sizes was represented in form of a histogram and morphology characterisation parameters (eccentricity, roundness and elongation) were used to describe the crystal habit but were not presented here.

Calibration was carried out at the beginning of each experimental run to allow estimation of the actual crystals size. The minimum detectable particle size was estimated from the width of the captured area and the camera horizontal resolution as shown in Equation 4.1.

$$L_{min} = \frac{Width\ of\ captured\ area}{Horizontal\ resolution} \tag{4.1}$$

At least 100 frames from each video were used in background estimation and about 300 crystals were counted and analysed for crystal size distribution and habit. The modal sizes and coefficients of variation (cv) were all calculated to describe each obtained CSD and eccentricity histograms and variance was used to describe the width of the distributions. The crystal size distribution histograms for different residence times were represented at a constant suspension temperature and those for various supersaturations were presented at a constant residence time.

The particle population densities were estimated by dividing the counted number of particles by the product of captured area and depth of field as illustrated in Equation 4.2. Size of the captured area was estimated from the height and width of the field of view and the magnitude of the pixel which was obtained from calibration. The depth of field was experimentally

determined by measuring the distance in which particles remained reasonably sharp on a graduated glass ruler in a direction perpendicular to the field of view.

$$n = \frac{number\ of\ particles\ counted}{area\ of\ field\ of\ view\ \times depth\ of\ field} \quad 4.2$$

The obtained number was converted to specific particle density per micron by further dividing the obtained number by the bin size (Appendix 4) and this was plotted against the particle size as the particle size distribution. Algorithms used are presented in the Appendices. The term particle was adopted for ice because it was difficult to distinguish between a crystal and an agglomerate.

4.3 Experimental Procedure

The storage tank was filled with 10L of 3.79 to 5 wt % synthetic sodium sulphate aqueous solution and a magnetic stirrer mixed the contents of the storage vessel for at least 15 minutes. This ensured dissolution of any salt crystals before the solution was pumped into the pre-cooler. Part of the feed solution was transferred from the storage tank to fill up the pre-cooler and crystallizer using peristaltic pumps. The crystallizer solution was agitated for 15 minutes, at 73 rpm, to homogeneously mix the solution at 25^{o}C before the coolant was introduced from the GR 150 thermostatic unit.

The well mixed crystallizer solution was gradually cooled from ambient temperatures to -2.2 ^{o}C at which either approximately 0.1 g of sodium sulphate decahydrate or ice seeds were added to initiate nucleation. After nucleation, the solution temperature, monitored by a Pt 100 thermocouple increased but was adjusted to temperatures between -1.1 and -1.2 ^{o}C by lowering coolant temperature. When close to 20% solids content had formed, the process was switched to continuous mode by starting the salt product withdrawal pump. Simultaneously, the feed solution was introduced into the crystallizer at a temperature 1-3 ^{o}C above the operating condition. The refrigerant inlet temperature was adjusted, to remove sensible heat added into the system by feed solution introduction, in order to restore the crystallizer bulk suspension temperature.

The salt product slurry was pumped from the bottom of the crystallizer and recycled to the storage vessel where the salt was re-dissolved with the aid of a magnetic stirrer. Ice slurry overflowed from the crystallizer top into an open tank where ice quickly melted and

accumulated as a solution which was recycled back to the storage tank. The process was allowed to operate for durations of at least 8τ which was deemed sufficient for attainment of steady state conditions with respect to product size and shape (Sha et al., 1996; Swenne, 1983).

A Mikrotron (MC1363) CMOS digital camera, with a resolution of 1280 x 1024 pixels, was used to capture images of crystals after steady state had been attained. The images were then loaded into MatLab R2011b®, processed and analysed in order to extract crystal size distribution and shape. The salt morphology was also determined by viewing under a microscope (Olympus BX 501). Three samples of the mother liquor solution were collected from the crystallizer, at steady state using a syringe, and analysed for sodium ion concentration using Atomic Absorption Spectroscopy.

The effect of residence time on product quality was investigated by repeating the procedure at three different feed solution flow rates at a relatively constant bulk suspension temperature. This was carried out for both 5 and 3.79 wt% feed solution as summarised in Table 4.1.

Table 4.1: Operating conditions for residence time investigations

Feed conc (wt%)	τ (min)	Tsus (°C)
5.00	10	-1.20
5.00	20	-1.20
5.00	30	-1.20
3.79	20	-1.11
3.79	30	-1.11
3.79	45	-1.11

Experiments were then conducted, in triplicates, at three different crystallizer operating temperatures and a constant feed flow rate corresponding to a nominal holding time of 30 minutes. An aqueous feed solution of 3.79 wt% sodium sulphate was employed for the investigations and the same experimental procedure was employed for each of the bulk suspension temperatures shown in Table 4.2.

Table 4.2: Operating conditions for supersaturation investigations

Feed conc (wt%)	τ (min)	Tsus (°C)
3.79	30	-1.10
3.79	30	-1.15
3.79	30	-1.20

5 Results and Discussion

In this section results of the experimental investigations conducted as detailed in Chapter 3 are presented and interpreted. Feed solutions of 3.79 and 5 wt% sodium sulphate aqueous solutions were employed in the experiments and the results are divided into two sections. The chosen compositions represented solutions of eutectic and hyper-eutectic sodium sulphate concentrations.

5.1 Cooling crystallization of 5 wt% Na_2SO_4-H_2O solution

The effect of residence time on the crystal size distribution and morphology of sodium sulphate decahydrate was investigated in the first set of experiments in which only salt was produced from a 5 wt% aqueous solution. As detailed in the experimental section, the crystal size distribution was obtained from the processed final binary image such as illustrated in Figure 5.1.

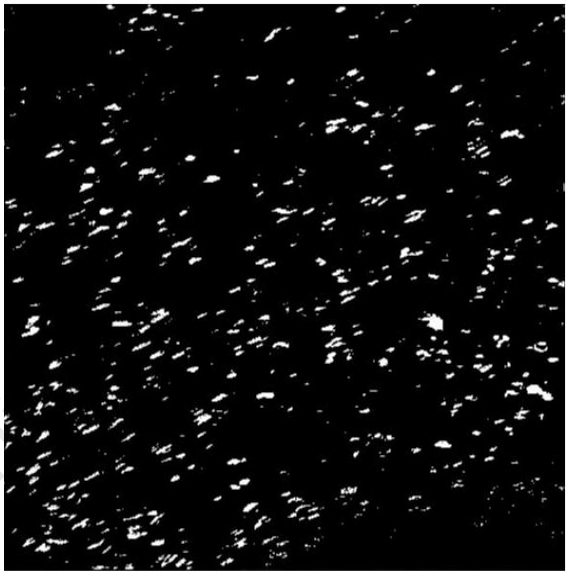

Figure 5.1: Binary image of Na_2SO_4. 10 H_2O crystals at τ = 10 mins

A number based crystal size distribution was obtained using an algorithm developed in Matlab R2011b® and the length of major axis was used to characterise the crystal size of the rod-like crystals observed. About 10 images were randomly chosen from an acquired batch of 100 frames, processed and analysed for crystal size distribution. Figure 5.2 illustrates CSDs of sodium sulphate decahydrate obtained from three experimental runs conducted at identical residence times of 10 minutes and operating suspension temperature of 0.4 °C. Aqueous feed

solutions of 5 wt% sodium sulphate composition were used in all the repeats and CSDs extracted from images captured after steady state conditions had been attained.

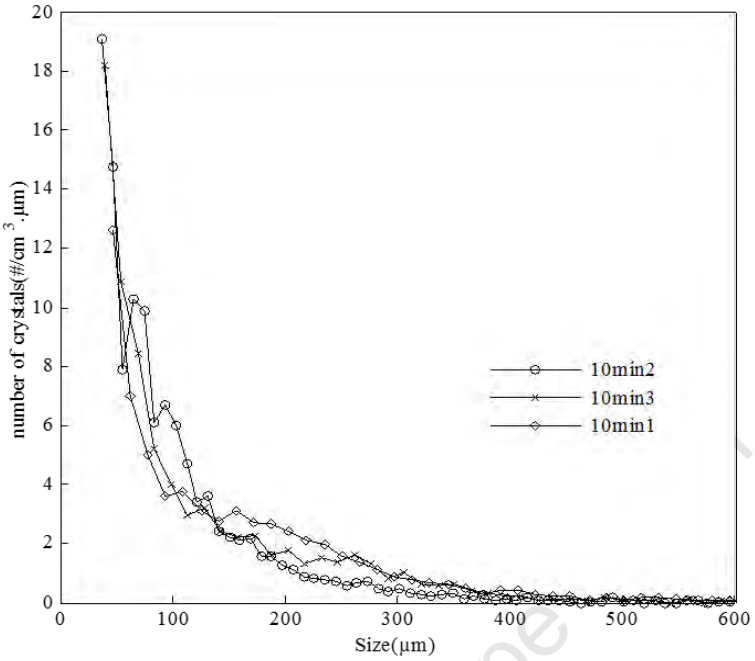

Figure 5.2: CSD for $Na_2SO_4.10H_2O$ crystals at τ = 10 minutes

Crystal size distributions presented in Figure 5.2 are all skewed towards the small crystal size range and showed similar crystal population densities for sizes larger than 400 μm. Crystals smaller than 30 μm were not measured due to experimental limitations regarding the smallest detectable size and increased inaccuracies in determining the population density of small crystals. However reproducibility in the crystal population densities was poor between 100 and 300 μm with experiment 10min1 showing slightly higher population densities of crystals between 150 and 250 μm than those observed for the other experimental runs. These differences were considered to be insignificant statistical random variations in the population density due to the dynamic orientations of the crystals due to mixing and were not associated with any other physical phenomena occurring in the crystallizer.

The shapes of the curves illustrated in Figure 5.2 indicated the existence of a similar dominant crystal size even though this was not determined due to limitations stated above. Measurements of the filtered salt product sizes using an optical microscope showed that this peak was very close to the maximum indicated by the highest point in the above curves as shown in Appendix 5.

All the CSDs showed bi-modal behaviour although this is emphasised in experiment 10min2 and suppressed in the other two runs. Large population densities of fine crystals, Figure 5.2, were attributed to uncertainty in counting the number of small crystals. The first 'projected' peak shown by the three crystal size distribution curves in Figure 5.2 were attributed to crystals with lengths extending into the third dimension of the field of view. The second maximum showed the dominant size of crystals whose full lengths were captured and this was assumed to be closer to the true dominant particle size of the crystal population.

5.1.1 Effect of residence time on CSD

The nominal residence time of the slurry in the crystallizer was then altered to 20 and 30 minutes by varying the feed flow rate at a relatively constant bulk suspension temperature of 0.4 °C. Experiments for all the three residence times were conducted in triplicates as described for 10 minutes and these were combined into 'composite curves' as shown in Figure 5.3, to allow an initial qualitative comparison of the crystal size distributions of the produced mirabilite. The distributions show the relative abundance of each crystal size interval.

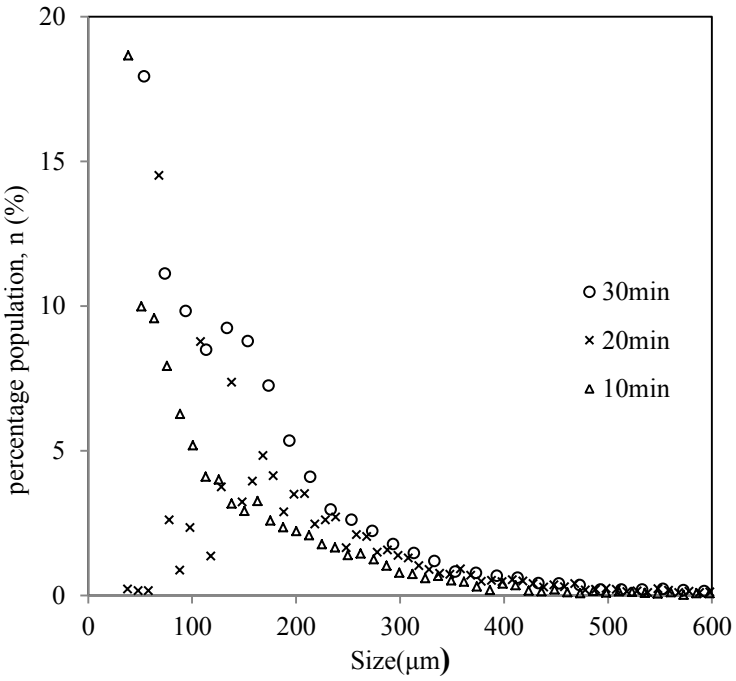

Figure 5.3: Variation of $Na_2SO_4.10H_2O$ CSD with residence time at 0.4 ^oC

All three CSDs showed predominance of small crystals with the size distribution obtained for 30 minutes lying to the extreme right of the three curves. The CSD obtained at 20 minutes residence time largely remained in between the curves for 10 and 30 minutes but crossed the

one for 10 minutes at smaller sizes. Comparable abundances of crystals below 100 μm were observed at 10 and 30 minutes while a relatively low abundance can be seen for 20 minutes. A log-normal distribution function described the CSD obtained at 20 minutes.

The three curves were characterised by 68%, 61% and 71% coefficients of variation for 10, 20 and 30 minutes respectively. A quantitative comparison of the crystal size distribution was made based on the mean crystal size obtained at each of the residence times. Mean crystal sizes obtained for the three residence times are summarised in Figure 5.4.

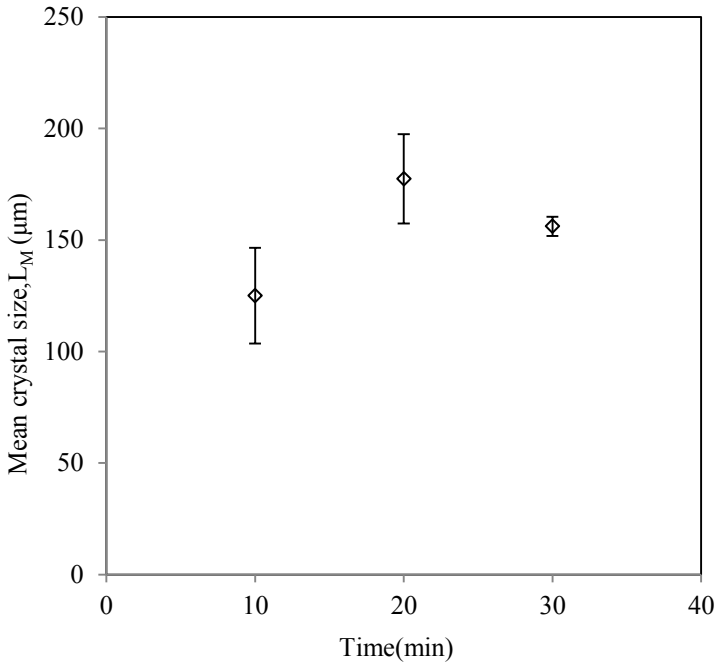

Figure 5.4: Mean crystal size variation with residence time

Increasing the nominal residence time from 10 to 20 minutes at a suspension temperature of 0.4 °C enhanced the mean crystal size of the product $Na_2SO_4.10H_2O$. Further increase in residence time to 30 minutes resulted in a slight decrease in the mean crystal size from 177 μm to 156 μm.

The increase in the mean crystal size with increase in residence time from 10 to 20 minutes was attributed to more time for growth at a longer residence times. This behaviour is consistent with a class II (fast growth) system with a relative kinetic order greater than 1 (Youngquist & Randolph, 1972; Mullin, 2001; Jones, 2002). Increasing the holding time for such a system reduces supersaturation which suppresses nucleation while promoting growth of the few crystals formed. Operating at longer retention times allowed more time for

crystallization of sodium sulphate from the solution resulting in lower supersaturation. This significantly reduced the nucleation rate, which has a stronger dependence on supersaturation than growth. It is notable that at lower supersaturation the growth is slower but this was compensated by a relatively longer duration in the crystallizer.

The observed increase in the mean product size (125 to 177 μm) was slightly larger than expected on doubling the nominal residence time from 10 to 20 minutes. Since no secondary size enlargement process was visually observed during the experiments, an overestimation could have arisen from experimental errors or image processing. A slight decrease in the mean size observed on increasing residence time to 30 minutes was due to attrition which generated a lot of fine crystals. Thus, a higher population density of crystals of 54 μm were observed at 30 minutes compared to 20 minutes, as shown in Figure 5.2, and this lowered the final mean crystal size.

Operating at 30 minutes nominal residence time using a 2L crystallizer resulted in very low flow rates which led to inefficient product removal due to low drag force on the crystals by the product stream. This further increased the residence time distribution of the solids in the crystallizer with the fraction of solids spending longer times actively contributing towards the formation of fine particles. Overall, the enhanced mean size estimated at 30 minutes, in comparison to the size at 10 minutes, represented a modest size enlargement which was ascribed to prolonged growth process at longer residence time.

At short residence times small crystals dominated the population due to limited time for growth to reach larger sizes. Secondly, high supersaturation, characteristic of short residence times (Kougoulos et al., 2005; Jones, 2002), stimulated a higher nucleation rate which predominated over growth rate. This produced large quantities of nuclei which provided a high surface area for growth but only a small increase in the characteristic size of each individual crystal. While the growth rate is understandably high at high supersaturation, this could not match the nuclei generation rate hence the observed high frequency of small crystals in the product.

The heat removal rate required to maintain the suspension bulk temperature at high flow rates is correspondingly high and this increased the rate of supersaturation generation in the crystallizer. In order to match the rate of supersaturation creation, the system responded by forming a large nuclei population which increased the surface area for growth. However, this

effect was expected to be less dominant during the crystallization of mirabilite compared to the influence of higher concentration at short residence times.

5.1.2 Residence time and morphology

As illustrated in Figure 5.5, no observable change in crystal morphology was realised upon increasing residence time from 10 to 30 minutes at a suspension temperature of 0.4 °C. A mixture comprising a large percentage of rod-like crystals and small percentage of small circular crystals were observed at 10 minutes and no significant change was realised when the nominal residence time was increased to 20 minutes.

(a) T =10 minutes

(b) T = 20 minutes

(c) T =30 minutes

Figure 5.5: Images showing $Na_2SO_4.10H_2O$ at different residence times and constant temperature of 0.4 °C

Further lengthening of residence time to 30 minutes only led to a slight increase in the thickness of the rod like crystals but no observable change in the proportional abundance of the crystals was observed. However, the increase in the thickness of the crystals was not detectable when shape description using elongation and eccentricity was tried. This behaviour was attributed to short residence times which were inadequate for any marked change in morphology. As can be clearly seen in Figure 5.5, crystals had no well-defined shapes except at 10 minutes where rod-like crystals were visually observed during experiments. This was due to damage on the faces of crystals as a result of collisions with the crystallizer walls, the impeller and scrapers and possibly no full view of the crystals since they were in motion.

Growth in the c-axis direction was high at short residence times hence the dominance of longer crystals. This suggested that growth along the c-axis is favoured at high supersaturation compared to growth in the a_1 and a_2 directions (Figure 2.9). The slight increase in crystal thickness with increase in residence time and presence of 'circle' like polyhedrons meant that growth in the latter directions increased with decreasing supersaturation. However the increase was insignificant as suggested by elongation factor which showed invariance with increase in residence time.

5.2 EFC of 3.79 wt% Na_2SO_4-H_2O system

An aqueous feed solution of 3.79 wt% sodium sulphate was employed for investigations at eutectic conditions. As a result of simultaneous crystallization of both ice and sodium sulphate decahydrate, the steady state residual concentration of sodium sulphate in the mother liquor varied with residence time as shown in Figure 5.6.

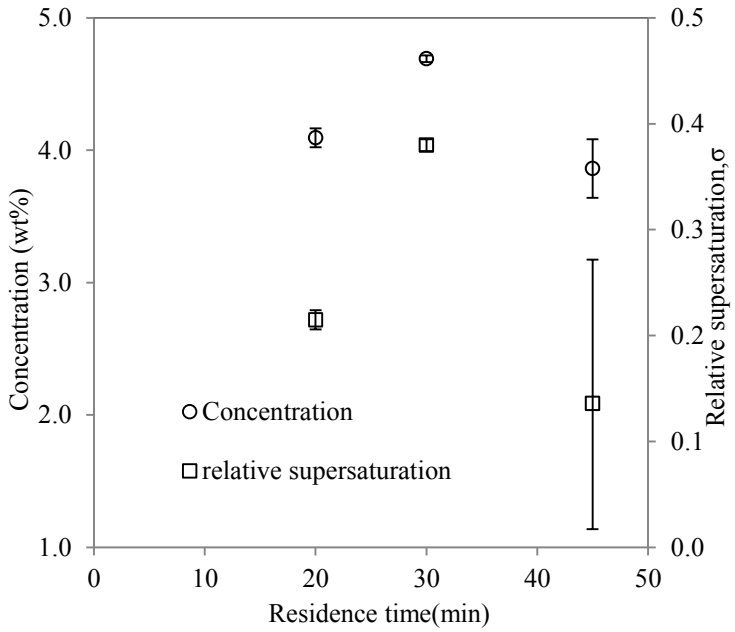

Figure 5.6: Supersaturation variation with residence time

As shown in Figure 5.6, the residual sodium sulphate concentration in the mother liquor increased and moved further away from the eutectic composition when residence time was increased from 20 to 30 minutes. Further increase of the nominal residence time to 45 minutes, however, resulted in a steady state composition which was very close to the eutectic value. The measured concentrations of Na_2SO_4 were used to estimate relative supersaturation with respect to mirabilite, using Equation 2.3. An arbitrary value obtained from extending the solubility line (Himawan, 2005) was used as the equilibrium value in computing the relative supersaturation.

The increase in the residual Na_2SO_4 concentration in the mother liquor on increasing the nominal holding time from 20 to 30 minutes was unexpected as the simultaneous crystallization of salt and ice would maintain the eutectic composition. Observed concentrating effect by solvent removal, under eutectic conditions, suggested faster crystallization kinetics for ice than the corresponding salt rates. Slower salt kinetics were attributed to the formation of the decahydrate whose nucleation kinetics are slow (Steiger & Asmusen, 2008) due to the activation enthalpy necessary for incorporation of water molecules into the hydrate unit cell (Genkinger & Putnis, 2007). However, since secondary nucleation is dominant in continuous processes, relatively faster kinetics would be expected and possibly the increase in concentration rather suggested cyclic crystallizer behaviour. The

removal of ten water molecules per unit of hydrate formation lessened the dilution effect and might have contributed towards the observed behaviour.

Increasing the average residence time to 45 minutes caused the operating point to move towards the eutectic point. This was attributed to dilution of the solution prompted by sodium sulphate decahydrate crystallization. A longer residence time was probably enough for sodium sulphate removal to counteract the concentrating effect imposed on the system by ice crystallization. The removal of the ice through crystallization possibly increased supersaturation, with respect to mirabilite, to a very high value during the transient state. This resulted in higher salt crystallization rates which forced the operating point to migrate towards the eutectic composition at steady state. A similar behaviour of mirabilite was observed by Rodriguez-Navarro and co-workers (2000) though in a different set up and not at eutectic conditions.

The behaviour shown in Figure 5.6 was attributed to faster solvent removal rate, by ice crystallization, at shorter holding times of 20 and 30 minutes which concentrated the solution thus increasing salt supersaturation. This meant a corresponding decrease in supercooling driving force for ice formation with increasing residence time. The maximum observed in the trends illustrated in Figure 5.6 suggested the existence of a threshold supersaturation at which the crystallization rate of sodium sulphate counteracted the concentrating effect of solvent removal and moved the steady state operating point towards the eutectic point. This depletion of sodium sulphate from the solution raised the ice melting temperatures, enhancing supercooling at a constant suspension temperature. The driving force for ice crystallization, which was defined as the deviation from the melting point corresponding to the steady state bulk solution sodium sulphate concentration, was in the order of 0.01 ^{o}C magnitude and difficult to measure.

At 45 minutes the operation of the 2L crystallizer approached that of a batch mode and the withdrawal rate dropped resulting in a higher magma density of sodium sulphate decahydrate in the crystallizer. This increased the specific surface area available for growth hence consumption of supersaturation and movement of the operating point towards the eutectic point.

5.2.1 Effect of residence time on particle size

Experiments in which the average crystallizer holding time was varied by adjusting the feed flow rate were conducted at a constant crystallizer operating temperature of -1.11°C. The

quality of the produced ice was measured in terms of particle size distribution and morphology. Particle size measurements were conducted after attainment of steady state and the equivalent circle diameter, evaluated from the 2-D projected area of particle images, was used to characterise particle size of the ice product.

Three identical experiments were run for each of the three residence times, in order to check reproducibility. Figure 5.7 shows three graphs summarising particle size distributions of the ice product obtained from three experimental runs conducted at 30 minutes average residence time and isothermal operating temperature of -1.11 °C.

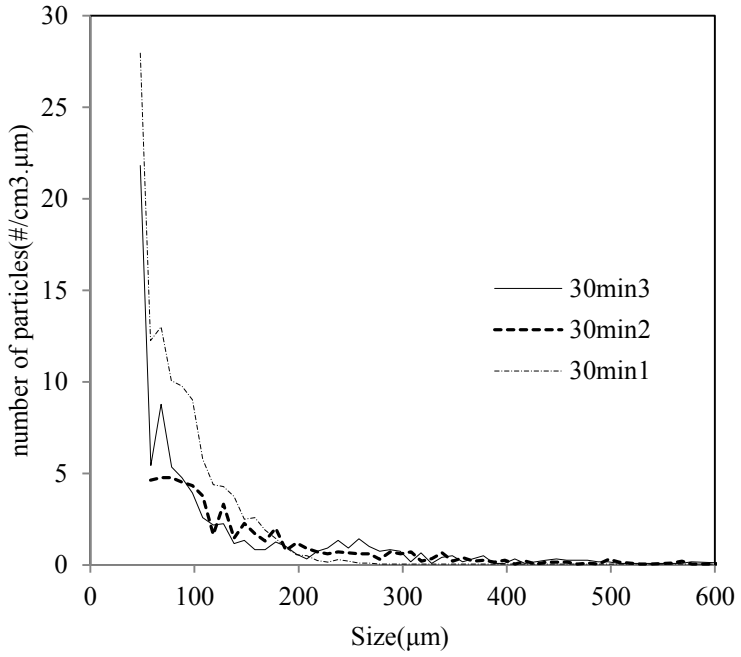

Figure 5.7: Ice PSD at τ = 30 minutes and supercooling of 0.01 ^{o}C

The particle size distributions show predominance of particles with sizes between 48 and 58 µm. A similar dominant particle size of 52 µm was estimated for experimental runs 1 and 3 while a slightly larger size of 68 µm was measured for run 2. Corresponding coefficients of variation for the three particle size distributions were estimated to be 51%, 48% and 65%. While both experimental run 1 and 3 showed similar ice dominant particle sizes of 52 µm, they showed very different particle population densities between sizes of 56 and 168 µm. Experimental run 1 showed the highest particle number density in the same size range while the ice particle concentration for the second run remained mid-way between corresponding values for runs 1 and 3 in the particle size range of 78 and 200 µm.

The shapes of the particle size distribution curves were similar for all the three experimental runs and generally a large concentration of particles with sizes between 48 and 100 μm was observed. A high population density of such sizes in the crystallizer was possibly an indication of the classification effect caused by preferential discharge of larger ice particles into the top separation compartment due to larger buoyancy forces consistent with observations by Wey and Estrin (1974). Although this effect is highly undesirable from the particle size measurement perspective, it could be an indication of good gravitational separation. The particle size distributions obtained for all the three experimental runs showed very small population densities for crystals larger than 600 μm. Poor reproducibility of fine particle concentrations was attributed to ambiguity in counting smaller particles and partly to uneven illumination which produced darker regions on the images.

Steady state particle size distributions of the ice product were also obtained for average crystallizer holding times of 20 and 45 minutes at a reasonably constant bulk suspension temperature of -1.11°C. These are presented in Figure 5.8 for the three residence times of 20, 30 and 45 minutes.

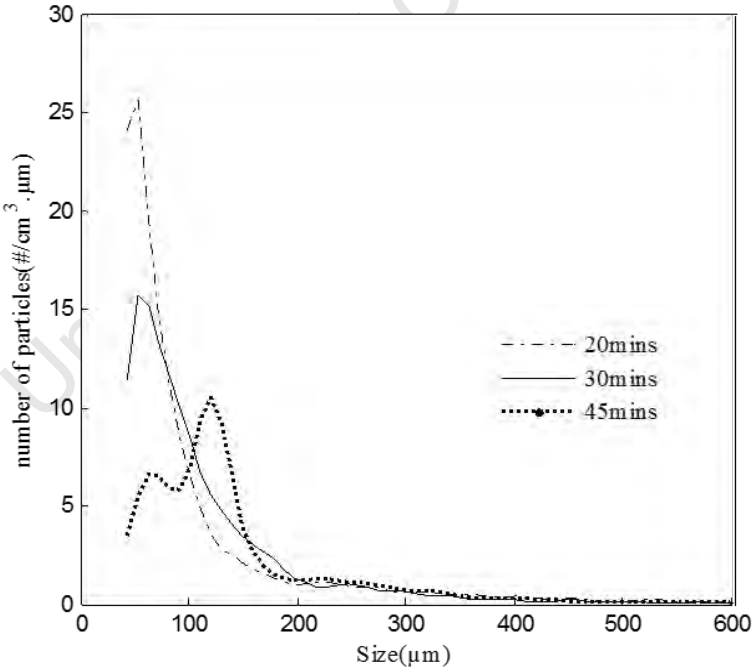

Figure 5.8: Ice PSD for τ = 20, 30 and 45 minutes at -1.11 °C

Particles of 52 μm dominated the ice particle size distribution at a nominal residence time of 20 minutes, as shown in Figure 5.8, and the distribution was described by cv of 55 %. Characterized by a very narrow peak, the PSD curve showed an initial sharp drop in the

specific population density of particles larger than the dominant size and a small peak at a particle size of around 250 μm. A similar dominant particle size of 57 μm was observed at 30 minutes and a cv of 55 % described the width of the distribution. Operating at 45 minutes residence time resulted in a wider particle size distribution with a low height and two distinct peaks. Estimated statistics for the obtained size distribution were 118 μm for the dominant particle size and a cv of 58%. The variation of the former with residence time is summarised in Figure 5.9.

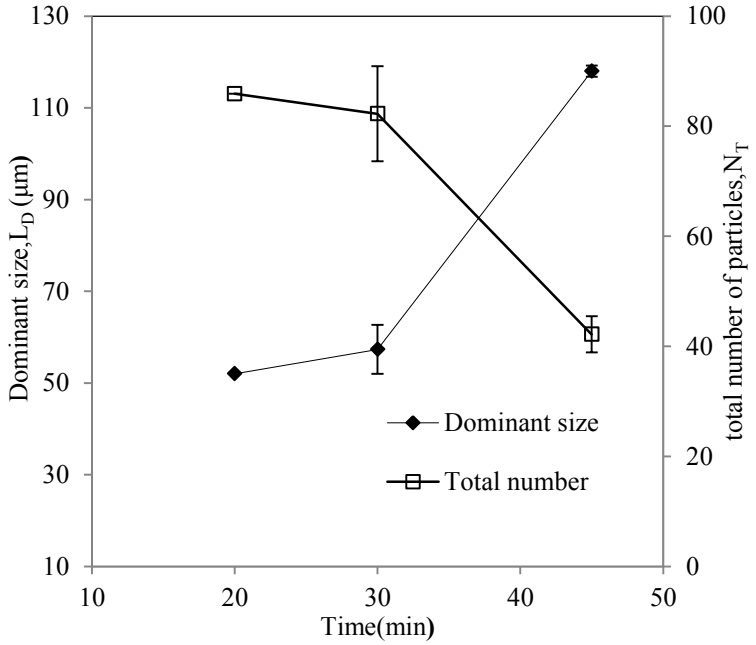

Figure 5.9: Variation of the dominant ice particle size with residence time

A general increase in the dominant particle size was observed upon increasing nominal residence time from 20 to 45 minutes at a constant suspension temperature. The dominant ice particle size increased from 52 μm at 20 minutes to 118 μm at 45 minutes while an opposite trend was observed in the corresponding particle population density which decreased with increase in the nominal residence time. However, only a small increase in the dominant ice particle size and corresponding decrease in the number density was observed on increasing the average holding time from 20 to 30 minutes.

The behaviour shown in Figure 5.9 was attributed to more time for growth as residence time increased. Although growth rate was relatively higher at 20 minutes, this did not produce larger particles due to a very high population density of fine crystals and inadequate time for growth and or dissolution. A high magma density predominated by fine crystals provided a

large surface area per unit mass resulting in only a marginal increase in the dominant size (52 to 57 μm) upon increasing nominal holding time to 30 minutes. This small increase in the dominant particle size upon increasing residence time from 20 to 30 minutes indicated that growth became slightly more important than nucleation as the level of supercooling decreased. Thus a fraction of particles obtained at 30 minutes occupies a region to the right of PSD for 20 minutes in Figure 5.8.

While the rates of both nucleation and growth diminished with decreasing flow rate, the former, being a stronger function of supersaturation (Wey & Estrin, 1974; Ulrich & Stelzer, 2011), dropped more rapidly than the latter, as supersaturation decayed with increasing residence time. Thus, relatively less number of particles formed at 30 minutes and the slight increase in the dominant size was due to a combination of slightly longer time for growth and less surface area for mass deposition. The small increase however, indicated that the nucleation rate was still high and this was attributed to high rates of secondary nucleation buttressed by ice mechanically sheared off crystallizer walls by scrapers and enhanced inter-particle collisions in the bulk suspension.

The largest dominant size obtained at an average residence time of 45 minutes was attributed, partly to longer times for growth and the occurrence of secondary processes of recrystallization in the form of Ostwald ripening. Increasing average residence times allowed suspended ice particles more time for growth and or dissolution in the bulk suspension as dictated by their individual sizes and supercooling in the ambient bulk solution (radius of curvature effect). Thus, fewer crystals, whose growth rates outweighed dissolution, provided surface area for mass deposition while smaller crystals melted.

The latent heat of crystallization rejected by the growing suspended particles actually promoted the dissolution of smaller crystals. However, it is important to realise that this cannibalistic tendency of relatively large ice crystals to grow at the expense of smaller ones was limited by the simultaneous crystallization of sodium sulphate, which opposed the migration of the ice-solution system towards equilibrium.

The variation of the mean particle size with residence time showed a similar trend to that exhibited by the dominant particle size as shown in Figure 5.10.

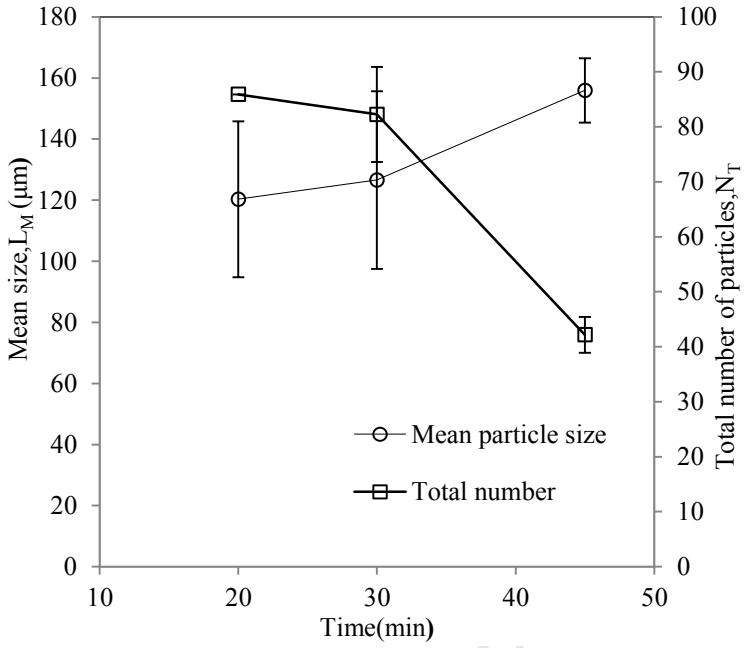

Figure 5.10: Variation in mean particle size of ice with residence time

The increase in the mean size shown in Figure 5.10 is consistent with findings by Russell and co-workers (1999) who reported a decrease in the average particle size with increasing throughput in an ice-cream manufacturing freezer. Although longer durations in the crystallizer allowed more time for growth, the increase in the mean particle size on changing residence time from 30 to 45 minutes was unrealistically large for less than two-fold increase in residence time. This suggests the occurrence of secondary recrystallization phenomena in the crystallizer as the nominal holding time increased at constant temperature.

The bi-modal particle size distribution obtained at 45 minutes holding time (see Figure 5.8), strongly supports the occurrence of both primary and secondary size enlargement processes with the latter responsible for the peak observed at 118 μm. It was speculated that a combination of growth and agglomeration led to the particle size distribution observed at 45 minutes nominal holding time. The increase in supersaturation induced by mirabilite crystallization supported the survival of small crystals (increased collision frequency) and building of crystalline bridges between ice particles.

The large population density of smaller crystals observed at 20 minutes resulted from short durations spent by particles in the bulk suspension, which was inadequate for crystals to grow

to large sizes. While kinetic rates of both nucleation and growth are high at short residence times, due to higher levels of supersaturation, the relative kinetic rates between the two determines the stationary particle size distribution. It is evident from the observed high solids fraction at 20 minutes that nucleation, which is a stronger function of the driving force and was enhanced by ice scraped off the colder crystallizer walls, outweighed growth at short holding times. This is consistent with observations by Russell and co-workers (1999) and Drewett and Hartel (2007) in ice manufacturing freezers.

The potential ice nuclei deposited in the bulk suspension would either grow or dissolve as dictated by the size of the particles. The comparatively high supersaturation, prevailing at 20 minutes residence time, supported the survival of most of the products of mechanical and hydrodynamic shear forces, responsible for secondary nucleation in the bulk, through reduction of the critical radius of the nuclei (Mersmann et al., 2001). This resulted in the smaller dominant and mean particle sizes, as illustrated in Figure 5.9. This was exacerbated by limited recrystallization due to short durations of sheared ice in the crystallizer. The latter is consistent with observations by Russell and co-workers (1999) and Drewett and Hartel (2007).

Few, unusually large ice particles were also observed at 20 minutes during the experiments. This suggested the occurrence of agglomeration at short residence times. As explained by Russell and co-workers (1999), this is a dominant recrystallization mechanism in suspensions of high ice particle concentrations due to increased probability of inter-particle collisions. The high ice magma density, motivated by low crystallizer wall temperature and relatively high steady state supercooling, at 20 minutes, significantly contributed nuclei into the bulk suspension and sustained the survival of a large percentage of the nuclei, respectively. The latter further supported growth of interconnecting bridges between constituent units promoting agglomeration.

The lower particle population density observed at 30 minutes was attributed to the reduction in supercooling due to the increase in sodium sulphate concentration, which lowered the ice freezing point as noted by Barduhn and Huang (1987), Pronk (2006) and Margolis and co-workers (1971). A decrease in supercooling with increase in residence time resulted in a small decrease in the effective nucleation rate, which is highly sensitive to changes in supercooling, explaining the observed decrease in magma density on increasing residence time from 20 to 30 minutess under isothermal crystallizer operation.

The particle size distribution for 45 minutes exhibited the largest width of the three residence times while that of 20 minutes had the least variation. The increase in the coefficient of variation with increase in residence time at constant suspension temperature was mainly due to size enlargement and continual nucleation through secondary mechanisms. Constraints imposed by the mass conservation principles dictate a decrease in the population density of the particles and widening of the spread especially for a fast growth system. This is consistent with observations by Tahti (2004). Relatively finer ice crystals were deposited into the bulk, due to lower growth rate on the walls caused by slightly warmer coolant temperatures employed at 45 minutes at the same scraper rotational speed.

The growth rate, which is a function of supersaturation was used as an indication of the prevailing supercooling with respect to ice since the actual steady state driving force values were very low and difficult to measure as temperature approached equilibrium values. This, according to Youngquist and Randolph (1972), would be valid and reasonable for low order growth rate dependence on supersaturation. The growth rates along the basal plane were estimated from the slopes of semilog number size graphical plots for 20, 30 and 45 minutes as shown in Figure 5.11.

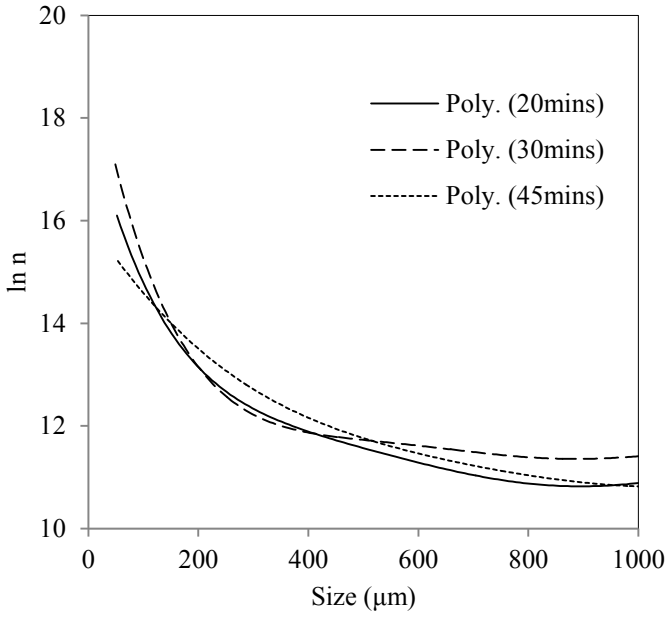

Figure 5.11 : Semi-log plot of number- size distribution

As can be seen in Figure 5.11, the graphs obtained by plotting the natural logarithm of the population density against particle size, were curved upwards. This suggested diffusion limited growth for sizes between 300 and 600 μm but linear sections of all the three curves

for fine crystals (below 200 μm) suggested a surface kinetics limited growth regime (size independent growth) for this size range. This violated some of the MSMPR assumptions. However, the method was employed inorder to compare the average growth rates at the different residence times based on the assumption that the cause of deviation from the MSMPR behaviour was common for the investigated residence times.

Estimation of the growth rate using models proposed by Margolis and co-workers (1971) and employed by Shirai and others (1986) would possibly improve the absolute values of the growth rates but with coefficients of determination (R^2) values greater than 0.84 the estimation using MSMPR was considered adequate for comparison purposes. The estimated growth rates estimated for the three residence times are shown in table 5.1.

Table 5.1: Variation of growth rate with residence time

Residence time (minutes)	Growth rate (μm/s)
20	0.057
30	0.050
45	0.090

The highest growth rate was estimated at 45 minutes while the lowest was at 30 minutes. This is consistent with supersaturation trends observed in Figure 5.6. The observed behaviour suggests a relative kinetic order greater than 1 (Randolph, 1965) for ice crystallization from a sodium sulphate aqueous solution compositions closer to eutectic values. In this case, supersaturation was mostly consumed by size enlargement than by new particle formation processes as residence time increased from 20 to 30 minutes resulting in an increase in the mean particle size. As such, increasing the nominal holding residence time allowed more time for growth hence size enhancement. A high growth rate at 45 minutes was due to uncharacteristically high supercooling caused by mirabilite crystallization which counteracted the decrease in the melting point at constant suspension temperature. Agglomeration effects could be responsible for this as well.

The power input per unit volume was kept constant by maintaining the stirrer and scraper speeds at constant values for all the different residence times investigated. It was assumed

that no significant change in mixing occurred due to changes in the feed flow rate as the turbulence level in the agitated crystallizer was already very high. Changing the feed rate rather altered the hydrodynamic force in the vertical direction hence the escaping probability of the particles. Appreciable drag forces might have increased the rate of product particles removal thus causing higher supersaturation to prevail at higher flow rates.

5.2.2 Effect of supersaturation on ice particle size

The production rate of a continuous crystallizer at a constant nominal residence time is adjustable through operating at different levels of supersaturation. However, altering supersaturation changes the particle size distribution and shape of the produced solids, which ultimately affects the efficiency of gravitational separation.

The quality of ice produced at three different operating bulk suspension temperatures at a constant average residence time of 30 minutes was observed. A 3.79 wt% sodium sulphate aqueous feed solution was employed and coolant temperatures were adjusted between -5.5 and -6.5 ^{o}C to achieve bulk suspension temperatures of -1.1, -1.15 and -1.20 ^{o}C. Corresponding supercoolings at these operating bulk suspension temperatures were estimated from the steady state residual mother liquor sodium ion concentration and melting temperatures predicted using OLI software. Figure 5.12 presents particle size distributions of the ice product obtained at -1.15^{o}C and 30 minutes nominal residence time.

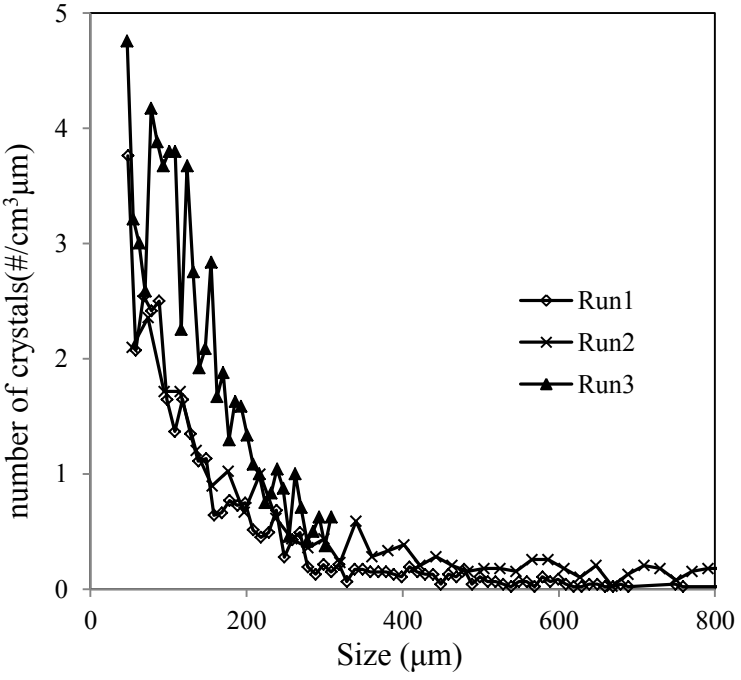

Figure 5.12: Ice particle size distribution at -1.15 °C and τ = 30 minutes

The particle size distribution obtained for experimental Run3 showed the highest crystal population density of particles between 48 and 200 μm while the other two repeats showed very similar particle population densities of sizes in the same particle size interval. These two runs further showed similar dominant sizes of 78 and 79 μm. The three particle size distributions presented in **Error! Reference source not found.** were then combined into a single distribution, using Matlab R2011b® for classifying particles into size intervals, to allow comparison with corresponding distributions obtained at bulk suspension temperatures of -1.11 and -1.20 ^{o}C. These PSDs, obtained at operating supercoolings of 0.01, 0.05 and 0.1 ^{o}C corresponding to slurry temperatures of -1.11, -1.15 and -1.20 °C respectively, are summarised in Figure 5.13. The distributions are all for an identical residence time of 30 minutes and the mentioned supercoolings were estimated from sodium sulphate concentration of the residual mother liquor at the mentioned operating temperatures.

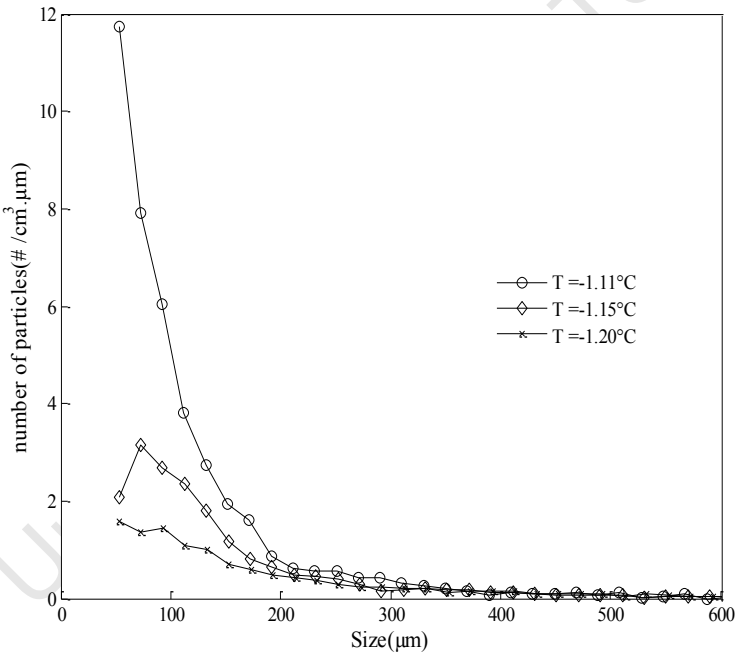

Figure 5.13 : Ice particle size variation with operating temperature

Operating at -1.11 °C produced the largest population density for particles of sizes between 48 and 200 μm as shown in Figure 5.13. An unexpectedly low particle population density was observed at the lowest temperature of -1.2 °C while that for -1.15 °C lies in between the former two. All the three particle size distributions showed similar population densities for particles larger than 400 μm and significant differences were observed at sizes below this value as shown in Figure 5.13.

Generally the particle population densities shown are very low compared to findings by Margolis and co-workers (1971) and in order to allow just comparison, the respective mean particle size were used. The lower population densities estimated at larger supercoolings resulted from poor illumination arising from relatively higher magma density, visually observed during experiments, and interference due to scale formation.

Figure 5.14 summarises mean particle sizes obtained at supercoolings of 0.01, 0.05 and 0.1°C, under a common residence time of 30 minutes.

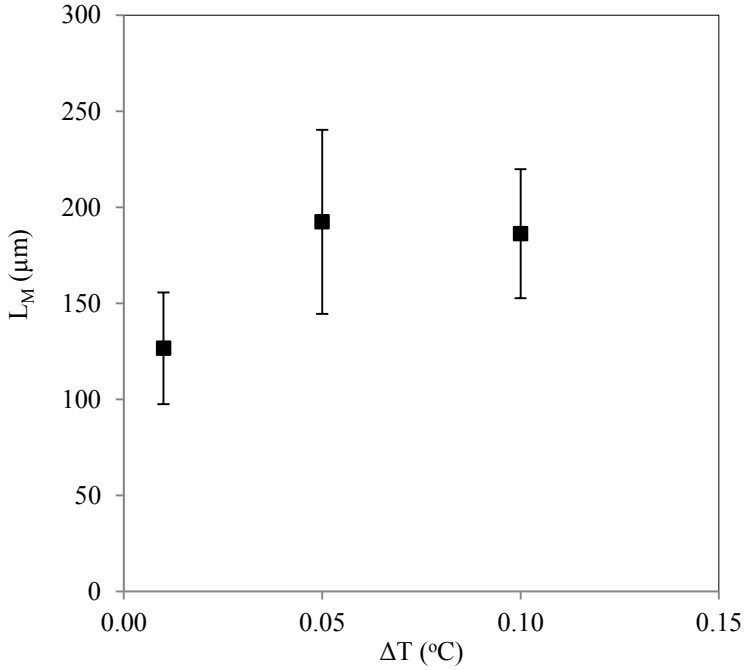

Figure 5.14 : Mean particle size variation with supercooling

As illustrated in Figure 5.14, the mean ice particle size increased from 127 µm at 0.01 °C to 192 µm at 0.05 °C and slightly dropped to 186 µm when supercooling was further increased to 0.10 °C. The variation in the mean particle size was largest at 0.05 °C and the least variation was observed at 0.01 °C. It can be clearly seen that the mean size obtained at 0.10°C was well within the limits of that obtained at 0.05 °C. This suggests that the mean particle size remained almost invariant on increasing supercooling from 0.05 to 0.1 °C.

The increase in the mean particle size with increase in supercooling, as illustrated in Figure 5.13, is inconsistent with findings by Drewett and Hartel (2007) and Alvarez and Myerson (2010), who observed a decrease in the mean particle size with increase in supercooling. While increasing supercooling enhances the rate of nucleation, as observed by

the mentioned workers, it can be reasonably argued that increasing supercooling from 0.01 to 0.1 °C was insufficient to induce primary nucleation in the bulk suspension. While primary nucleation produces large quantities of nuclei and suppress growth, secondary nucleation is also enhanced at higher supercoolings. This still points to a decrease in mean size with increasing supercooling which contradicts the behaviour illustrated in Figure 5.14.

The behaviour observed in Figure 5.14 was tentatively attributed to high supersaturation local to the colder crystallizer walls. This stimulated heterogeneous primary nucleation on the crystallizer wall surfaces, which, aided by the mechanical action of scrapers which sheared and discharged the formed ice into the bulk suspension, produced large quantities of potential ice nuclei. The ice slush, provided a large surface area which promoted growth (Jones, 2002) hence increase in the mean particle size. This however, would not exclude enhanced secondary nucleation in the bulk but an increase in mean size meant that consumption of supersaturation by growth on existing crystal surfaces outweighed the consumption of the same by nucleation. This complex interaction of nucleation and growth made it difficult to outrightly identify mechanisms which led to the trend observed in Figure 5.14.

Heat rejected by the primary growth of ice in the bulk suspension melted some of the sheared ice promoting an Oswald ripening type of growth. This, in addition to heat generated by friction (Vaessen et al., 2004; Drewett & Hartel, 2007), controlled the amount of ice forming on the crystallizer walls, thus regulating wall contribution towards the nucleation rate. This is consistent with Russell and co-workers (1999) who found that the wall condition had no significant contribution to the final crystal size distribution and emphasized the importance of recrystalllization processes in the bulk suspension on the final product size distribution. Turbulence created by scrapers constantly disturbed the formation of a stagnant layer close to the crystallizer walls by mixing this fluid with the bulk as noted by Vaessen and co-workers (2004). This meant constantly short contact time between crystallizer walls and relatively warmer 'fresh' solution from the bulk suspension, thus ensuring that primary heterogeneous and secondary nucleation on the wall surfaces remained modest. It was suggested that growth in the suspension was consequently promoted hence the increase in mean size illustrated in Figure 5.14.

However, the enhancement of particle size, illustrated in Figure 5.14, is significant and could not be solely attributed to primary growth especially in the presence of a high specific area of ice particles. Changing the operating temperature to a lower value possibly led to a change in

the dominant kinetic process. Lowering temperature in the interval investigated in this work (-1.11 to -1.2 °C), would not significantly increase the viscosity of the mother liquor and or surface integration kinetics hence was considered non-consequential in that regard. At warmer bulk solution temperatures, rates of growth-dissolution processes are enhanced and larger sizes were expected contrary to the trend observed in Figure 5.14. Since the feed hydrodynamic force was presumed constant at a constant nominal holding time of 30 minutes, any changes observed upon changing the operating temperature were exclusively attributed to supercooling. Thus changes in the hydrodynamic conditions were mainly caused by increase in the crystallizer magma density stimulated by higher supercoolings. A higher magma density slightly increased the solid phase residence time (Equation 2.15) at a constant product withdrawal rate. However, the purported increase in residence time was not adequate to explain the increase in the mean size from 126 to 192 μm in the small supercooling interval investigated.

This, suggests a change in size enlargement recrystallization mechanism from growth-dissolution to agglomeration, which is supported by high magma densities. Increased solid content in the crystallizer changed the hydrodynamics to conditions suitable for agglomeration of the formed crystals (see Figure 5.15).

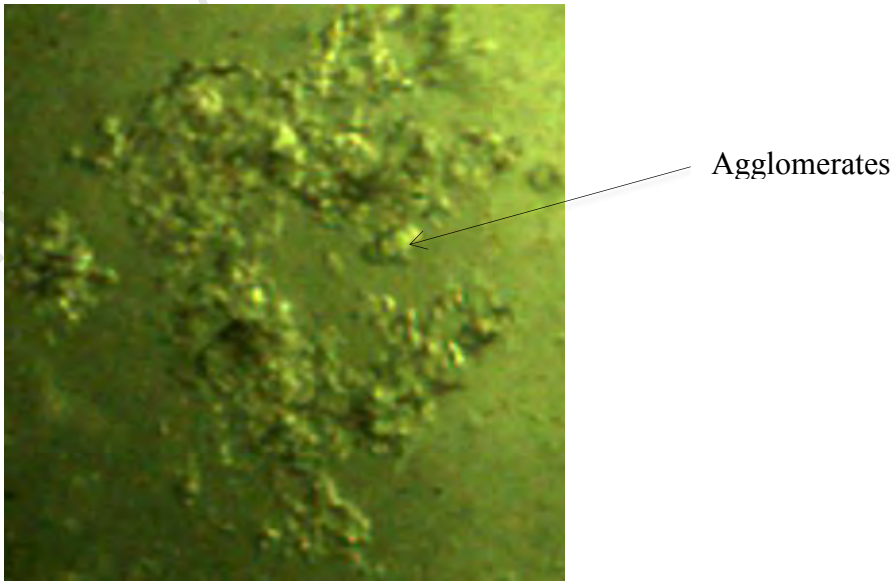

Figure 5.15: Agglomerates formed at -1.2 °C

Since mechanical energy input per unit volume was maintained, by running the stirrer and scrapers at relatively constant rotational speeds, higher magma density increased the inter-particle collision frequency hence the rate of agglomeration. In addition to this, higher solid

content increased the viscosity of the slurry and reduced the impact of disruptive forces therefore enhancing the cementation of the ice particles upon collision. This was further reinforced by crystallization of mirabilite which mutually generated supercooling for ice further supporting the construction of crystalline bridges between particles. The corresponding dominant particle sizes were looked at in order to further understand the mechanisms behind the observed trend. These are shown in Figure 5.17.

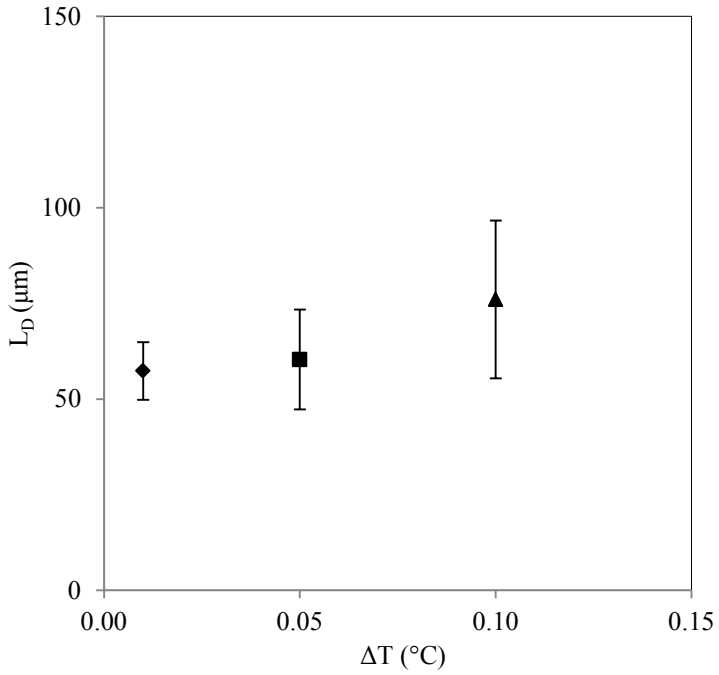

Figure 5.16: Dominant ice particle size variation with supercooling at τ = 30 minutes

A marginal shift in the ice dominant size was observed on changing supercooling from 0.01 °C to 0.1 °C. A dominant particle size of 57 µm was estimated at a supercooling of 0.01 °C and dominant particle size of 76 µm characterised the particle size distribution obtained at a supercooling of 0.1°C. A large increase in the mean particle size without a corresponding change in the dominant size meant that the generation of small particles remained high (seeding effect) but is an indication of increase in growth rate as well. The large specific surface area provided by the large amount of ice fines, resulted in only a marginal increase in size. This is an unexpected result since an increase in supercooling increases the rate of nucleation and instead of the obtained result; a decrease in the mean particle size was expected. The increase in dominant particle size suggested that the size of the actual discrete crystals increased marginally with increased supersaturation and further tests to verify this using a different method of measurement is recommended.

5.2.3 Effect of supercooling on morphology

The morphology of the ice product remained relatively invariant in the investigated range of supercooling. Figure 5.17 shows images captured during crystallization at 30 minutes residence time and -1.15°C operating temperature.

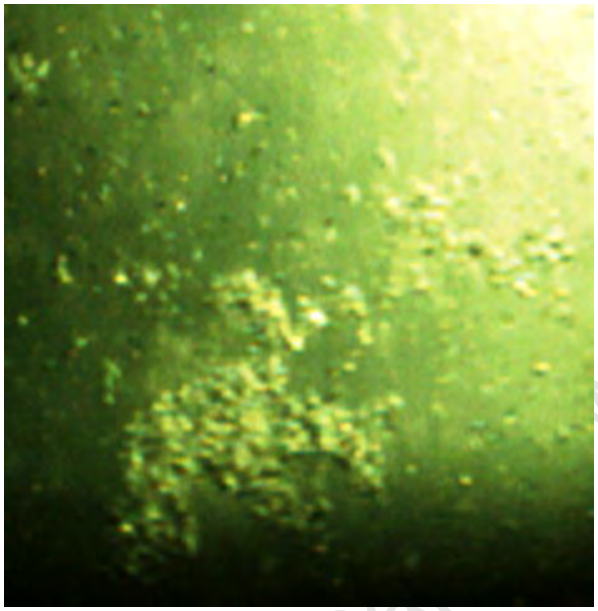

Figure 5.17 : Ice crystallizing out at -1.15 °C

Plate-like disks of ice crystals were formed between 0.01 and 0.1°C supercooling with particles becoming slightly elliptical as supercooling increased to 0.1^{o}C. Increasing supercooling to values higher than 0.1 °C indicated dendrites formation but operational difficulties excluded further investigations at higher supercoolings. The formation of disks meant that anisotropic growth of ice in the c-axis and a-axis directions occurred in the investigated supersaturation range. This is consistent with findings from previous work by Harriot (1967), Margolis and co-workers (1971) and who concluded that growth in the basal direction was faster than growth normal to the basal plane.

It could not be established whether the some of the apparently disk shaped particles were hexagonal or circular shaped using the method employed in this work. However the observed particle images, suggested that a mixture of plate-like and elongated ice disks were formed for all the supercoolings between 0.01 and 0.1 ^{o}C. The formation of disk shaped crystals meant that the growth rate along the basal plane was faster relative to that in the c-axis direction. Growth rates reported in the previous sections were all for growth in the a-axis and taking shape into account would allow estimation of growth kinetics in the c-direction.Lack

of significant change in morphology suggested no major change in the growth regime kinetics in the supercooling interval investigated.

5.3 Implications on EFC operation

In summary, it has been found that lengthening residence time at a constant eutectic crystallizer operating temperature enhances the mean particle size of the ice product without a significant change in the disk-like shape of ice crystals. The increase in mean size was attributed to more time for crystal growth and recrystallization at longer holding times. This is valid at low supercoolings ($\Delta T<0.1°C$) and the behaviour may not be extrapolated to higher supercoolings. It is important to note that increasing the feed flowrate in this case, results in the deterioration of the mean crystal size hence longer residence times, together with ageing tanks, should be integrated into an EFC process to produce larger crystals suitable for gravitational separation.

An increase in supercooling from 0.01 to 0.05 °C, at a constant residence time of 30 minutes, increased the mean particle size of the ice product but further increase to 0.1°C resulted in a slight decrease in the same. This suggests that the mean crystal size passes through a maximum if supercooling is increased at a constant nominal holding time. Thus, the production rate of solid products in a eutectic crystallizer can be increased in a narrow window of operation without a deterioration in the mean particle size. However, further increase in the production rate above a certain threshold, through increasing supercooling, results in the promotion of higher nucleation rates hence deterioration of the mean product size. Enhanced agglomeration, evident at high supercooling, would also increase impurity content of ice through increased entrapement of salt particles by the floating agglomerates.

6 Conclusions

The mean crystal size of $Na_2SO_4.10H_2O$ marginally increased with residence time in a cooling crystallization process but no change in morphology was observed. The increase was attributed to low supersaturation, at longer residence times which promoted growth over nucleation. Mean particle size of ice product increased significantly with increasing residence time between 20 and 45 minutes residence time at an isothermal crystallizer operating temperature of -1.11°C. The increase in the mean particle size was attributed to prolonged recrystallization at longer residence time which allowed enough time for Ostwald ripening.

Increasing the operating supercooling at constant overall residence time increased the mean particle size of the ice product. This was partly due to promotion of growth on the existing crystals and enhanced agglomeration rates at lower operating temperatures. A mixture of plate-like and round disks of ice were formed and this morphology remained almost invariant under the conditions investigated with only a few particles exhibiting elongated disk shapes. The formation of the latter was attributed to agglomeration of two or more particles especially at lower temperatures where this phenomenon became the dominant recrystallization mechanism.

The designed crystallizer operated at a maximum supercooling of order of 0.1 °C at nominal residence times of between 10 and 45 minutes. Above this supercooling agglomeration rate increased sharply as was visually observed and this produced an ice product which was difficult to separate. The nucleation rate was very high and this hampered the growth of crystals resulting in particle size distribution dominated by fine particle population density. High nucleation rate was due to contribution by secondary and heterogeneous nucleation mechanisms on the colder crystallizer walls.

7 Recommendations

Retention times longer than 45 minutes should be investigated and this requires a larger crystallizer volume and the size should allow the independent variation of residence times of the ice and salt product. Multi-tank crystallizers may potentially improve the shape of the product crystal size distribution. Further experiments should be conducted in which only the actual crystal size variation with residence time and supersaturation would be investigated.

Crystallizer designs with higher heat transfer surface areas should be explored in order to minimise the temperature driving force between the coolant and the crystallizer contents. Crystallizer materials of construction different from glass, which was employed in this study, should be employed in order to improve heat fluxes which directly affect the mass production rate at steady state conditions.

The classified product removal and fines destruction operating modes should be considered to improve ice product particle size distribution by selectively allowing different residence for product crystals based on size and promotion of growth through controlling the nucleation rate.

A Eutectic Freeze Crystallizer should be operated at low supersaturations to minimise the formation of agglomerates which compromises the ultimate water product purity. A maximum of 0.1 °C was determined for a 2 L glass crystallizer employed in this work above which the rate of agglomeration was visually observed to increase. Smooth operation of the crystallizer also require low solids content to minimise blockages of the product withdrawal ports.

The thresholding step of image analysis needs improvement to achieve better accuracy in the particle size measurement and minimise the loss of the objects of interest. Illumination of the captured area needs improvement and the use of crossed polaroids (due to birefringence properties of ice) should be instituted to improve ice particle detection. Furthermore, immobilisation of the product crystals may also improve the number of particles in focus. It is recommended that the digital imaging method be employed in conjunction with electrical zone sensing method for measurement of sizes below 30 μm to further improve the accuracy of size measurement over the whole range of particle size.

8 References

Aamir, E., 2010. *Population balance model-based optimal control of batch crystallisation processes for systematic crystal size distribution design*. PhD Thesis. Loughborough University.

Alvarez, A.J. & Myerson, A.S., 2010. Continuous Plug Flow Crystallization of pharmaceutical compounds. *Crystal Growth& Design*, 10(5), pp.2219-28.

Arellano, M.P., Aguillera, J.M. & Bouchon, P., 2004. Development of a digital video microscopy technique to study lactose crystallization crystallization in situ. *Carbohydrate Research*, 339, pp.2721-30.

Arellano, M., Benkhelifa, H., Flick, D. & Alvarez, G., 2012. Online ice crystal size measurements during sorbet freezing by means of the focused beam reflectance measuremnt(FBRM) technology.Influence of operating conditions. *Journal of Food Engineering*, 113, pp.351-59.

Barduhn, A.J. & Huang, J.S., 1987. Why does ice grow faster from salt water than fresh water. *Desalination*, 66, pp.99-106.

Brown, C.J. & Xiong-Wei, N., 2011. Online evaluation of paracetamol antisolvent crystallization growth rate with video imaging in an oscillatory baffled crystallizer. 11, pp.719-25.

Cook, K. & Hartel, R., 2010. Mechanisms of ice growth in ice cream production. *Comprehensive reviews in food science and food safety*, 9, pp.213-22.

Daudey, P.J., 1987. *Crystallization of ammonium sulphate- secondary*. Technical University of Delft.

Dirksen, J. & Ring, T., 1991. Fundamentals of Crystallization : Kinetic Effects on Particle Size Distributions and Morphology. *Chemical Engineering Science*, 46(10), pp.2389-427.

Drewett, E. & Hartel, R., 2007. Ice crystallization in a scraped surface freezer. *Journal of Food Engineering*, 78, pp.1060-66.

Fakatselis, T.E., 2002. Residence time optimization in continuous crystallizers. *Crystal Growth & Design*, 2(5), pp.375-79.

Garside, J., 1985. Review Article Number 15 industrial crystallization from solution. *Chemical Engineering Science*, 40(1), pp.3-26.

Genceli, F.E., 2008. *Scaling-Up Eutectic Freeze Crystallization*. PhD Thesis. Delft: Technical University of Delft Technical University of Delft.

Genceli, F.E. Gartner, R., Trambitas, D., Rodriguez M., & Witkamp, G.J. 2005. 3rd Generation Cooled Disk Column Crystallizer and A Skid Mounted Unit for Eutectic Freeze

Crystallization. Dresden, Germany, 2005. 16th International Symposium on Industrial Crystallization.

Genkinger, S. & Putnis, A., 2007. rystallization of sodium sulfate :supersaturation and metastable phases. *Environmental Geol*, 52, pp.329-37.

Han, C.D. & Shinnar, R., 1968. The steady state behaviour of crystallizers with classified product removal. *American Institute of Chemical Engineers*, 14(4), pp.612-19.

Harriot, P., 1967. The growth of ice crystals in a stirred tank. *American Institute of Chemical Engineers*, 13(4), pp.755-59.

Hattaka, H., 2010. *Effect of hydrodynamics on modelling and control of crystallization*. Lappeenranta, Finland.

Helt, J.E. & Larson, M.A., 1977. Effects of temperature on the Crystallization of Potassium Nitrate by Direct Measurement of Supersaturation. *AIChE*, 23(6), pp.822-30.

Himawan, C., 2005. *Characterization and Population Balance Modelling of Eutectic Freeze Crystallization*. Delft: Laboratory for Process Equipment, Delft University of Technology, The Netherlands.

Hossein, K. & Da-Wen, S., 2011. Water crystallization and its importance to freezing of foods:a review. *Trends in Food Science & Technology*, 22, pp.407-26.

Huige, N.J.J., 1972. *Nucleation and Growth of ice crystals from water and sugar solutions from continuous stirred crystallizers*. Eindhoven.

Jones, A., 2002. *Crystallization Process systems*. Oxford: Butterworth-Heinemann.

Jones, J. & Ulrich, J., 2006. Heat and mass transfer operations crystallization.

Kane, S., Evans, T.W., Brian, P. & A.F.Sarofim, 1975. The kinetics of the secondary nucleation of ice :implications to the operation of continuous crystallizers. 17, pp.1-14.

Kiani, H. & Sun, D.-W., 2011. Water crystallization and its importance to freezing foods :A review. *Trends in Food Science & Technology*, 22, pp.407-26.

Kougoulos, E., Jones, A.G. & Wood-Kaczmar, M.W., 2005. Estimation of crystallization kinetics for an organic fine chemical using a modified continous cooling mixed suspension mixed product removal (MSMPR) crystallizer. *Journal of Crystal Growth*, 273, pp.520-28.

Libin, Y., Du, J., Jianjun Y. & Sha, Z. n.d. Crystallization kinetics of sodium sulphate decahydrate in an MSMPR stirred crystallizer.

Margolis, G., K.Sherwood, T. & Brian, P.T., 1971. The perfomance of a Continuous well Stirred Ice Crystallizer. *Ind.Eng.Chem.Fundam.*, 10(3), pp.439-51.

Markov, I., 1995. *Crystal Growth for Beginners: Fundamentals of Nucleation, Crystal Growth and Epitaxy*. World Publishing Scientific Company Pte Ltd.

Mersmann, A., 2001. *Crystallization Technology Handbook*. Basel, Switzerland: Marcell Dekker.

Mersmann, A., Heyer, C. & Eble, a., 2001. Activated Nucleation. In A. Mersmann, ed. *Crystallization Technology Handbook*. 2nd ed. Marcel Dekker,Inc. pp.68-77.

Mina-Mankarios, G., 1988. *Crystallization kinetics of Sodium Sulphate in a salting out MSMPR crystallizer system $Na_2SO_4/H_2SO_4/H_2O/MeOH$*. Masters Thesis. Vancouver: University of British Columbia.

Mullin, J.W., 2001. *Crystallization*. Reed Educational and Professional Publishing Ltd.

Myerson, A. & Ginde, R., 2002. Crystals, Crystal Growth, and Nucleation. In *Handbook of Industrial Crystallization*. 2nd ed. Butterworth-Heinemann.

Nienoord, M. & Verdoes, D., 1999. Eutectic Freeze Crystallization simultaneous Recovery of Potassium Nitrate and Water from Industrial Stream. In *Industrial Crystallization*., 1999.

Petzgold, G. & Aguilera, J.M., 2009. Ice morphology: Fundamentals and technological applications in foods. *Food Biophysics*, 4, pp.378-96.

Pronk, P., 2006. *Fluidised bed heat exchanger to prevent fouling in ice slurry systems and industrial crystallizers*. PhD. Delft University of Technology.

Randall, D., 2010. *Development of a brine treatment protocol using Eutectic Freeze Crystallization*. Cape Town: Department of Chemical engineering,University of Cape Town.

Randolph, A.D., 1965. The mixed suspension ,mixed product removal crystallizer as a concept in crystallizer design. *AIChE*, 11(3), p.424.

Randolph, A.D. & Larson, M.A., 1971. *Theory of Particulate Processes : Analysis and Techniques of Continuous Crystallization*. New York and London : Academic Press Inc. Ltd.

Rawlings, J.B., Miller, S.M. & Witkowskit, W.R., 1993. Model Identification and Control of Solution Crystallization Processes. (32).

Reddy, S.T., Lewis, A.E., Witkamp, G.J, Kramer, H.J.M.& Spronsen, J. 2010. Recovery of $Na_2SO_4.10H_2O$ from a reverse osmosis retentate by Eutectic Freeze Crystallization technology. *Chemical Engineering Research and Design* , 88, pp.1153-57.

Ring, T.A., 1991. Kinetic effects on particle morphology and size distribution during batch precipitation. (65).

Rodriguez, P.M., 2009. *Physical aspects of a Scraped Heat Exchanger Crystallizers An application in Eutectic Freeze Crystallization*. Technical University of Delft.

Rodriguez-Navarro, C., Doehne, E. & Sebastion, E., 2000. How does sodium sulfate crystallize?implications for the decay and tesing of building materials. *Cement and Concrete Research*, 30, pp.1527-34.

Rodriguez, P.M., Ravelet, F., Delfos, R. & Witkamp, G.J., 2008. Measuremet of flow field and wall temperature distribution in scraped heat exchanger crystallizer. In *5th European Thermal-Sciences Conference, The Netherlands, 2008*. Eindhoven, 2008.

Russell, A., P.E.Cheney & Wantling, S., 1999. Influence of freezing conditions on ice crystallization in ice cream. *Journal of Food Engineering*, 39, pp.179-91.

Seckler, M., Verdoes,. & Witkamp, G., 2002. *Application of Eutectic Freeze Crystallization to Process Streams and Wastewater Purification*. Delfty,The Netherlands: Economy,Ecology and Technology.

Selvaduray, G., 2000. Ternary Phase Diagrams An introduction.

Sha, Z.L., Hatakka, M.L.-K. & Palosaari, S., 1996. Crystallization kinetics of potassium sulfate in an MSMPR stirred crystallizer. *Journal of Crystal Growth*, (166), pp.1105-10.

Shirai, Y., Kazuyuki Sakai, K.N. & Matsuno, R., 1986. Analysis of ice crystallization in continuous crystallizers based on a particle size dependent growth rate model. *Chemical Engineering Science*, 41(9), pp.2241-46.

Spronsen, J.V., 2010. *Reactions and separations in green solvents*. Technical University of Delft.

Starck, J.L. & Murtagh, F., 2002. *Handbook of Astronomical Data Analysis*. Springer-Verlag.

Steiger, M. & Asmusen, S., 2008. Crystallization of sodium sulphate phases in porous materials: the phase diagram Na_2SO_4-H_2O and the generation of stress. *Geochimica et Cosmochimica Acta*, 72, pp.4291-306.

Stepakoff, G. & Siegelman, D., 1973. Application of Eutectic Freeze Crystallization Systems to Industrial Waste Water Recycling. Washington D.C., 1973. Industrial Waste Water Reuse Conference.

Stepakoff, G., Siegelman, D. & Johnson, R.a.G.W., 1974. Development of a Eutectic Freezing process for brine disposal. (14).

Stocking, J.H. & King, C.J., 1976. Secondary Nucleation of Ice in Sugar Solutions. *AIChE*, 22(1), pp.131-40.

Swenne, A.D., 1983. *The Eutectic Freeze Crystallization of NaCl.2H2O and Ice*. Eindhoven: Geboren TE Eindhoven.

Tahti, T., 2004. *Suspension melt crystallization in tubular and scraped surface heat exchangers*. Wittenberg, Germany: Martin-Luther-Universität Halle-Wittenberg.

Treptow, R.S., 1993. Phase diagrams for aqueous systems. *Journal of Chemical Education*, 70(8), pp.616-20.

Ulrich, J. & Jones, M.J., 2006. Heat and mass transfer operations - crystallization. Oxford, UK: Encyclopaedia of Life Support Systems. pp.1-31.

Ulrich, J. & Stelzer, T., 2011. Crystallization. In *Kirk-Othmer Encyclopedia of Chemical Technology*. John Wiley and Sons.

Vaessen, R., Janse, J., Seckler, M. & G.J, W., 2003. Evaluation of the perfomance of a newly developed eutectic freeze crystallizer. *Institution of Chemical Engineers*, 81 (PartA), pp.1363-72.

Vaessen, R., Seckler, M. & G.J, W., 2004. Heat transfer in scraped eutectic freeze crystallizers. (47).

Vaessen, R., Seckler, M. & Witkamp, G.J., 2003. Eutectic Freeze Crystallization with an Aqueous KNO3-HNO3 Solution in a 100-L Cooled Disk Column Crystallizer. *Ind. Eng. Chem. Res.*, 42(20), pp.4874-84.

van der Ham, F., 1999. *Eutectic freeze crystallization*. Delft, Netherlands: Technical University of Delft.

Verbeek, B.J., 2011. *Eutectic Freeze on Sodium Chloride Analysis of a full experimental cycle*. Delft, The Netherlands: Laboratory for Process Equipment, Process & Energy, Technical University of Delft.

Verdoes, D. et al., 1997. Improved procedures for separating crystals from the melt. *Applied Thermal Engineering*, 17(8-10), pp.879-88.

Wey, J.S. & Estrin, J., 1974. The growth and nucleation of ice in a batch couette. *Desalination*, 14, pp.103-20.

Witkamp, G.J., Vriejenhoef, J.P., De Graauw, J. & Van der Ham, F., 2001. Crystallization of materials from aqueous solutions.

Youngquist, G.R. & Randolph, A.D., 1972. Secondary nucleation in a class II system: ammonium sulphate-water. *AIChe*, 18(2), pp.421-29.

Yu, 2007. Review paper recent advances in crystallization control an industrial perspective.

9 Appendices

9.1 Appendix 1

Salt CSD analysis

```
clear all
close all
clc
a = dir('J:\A2-R2\*.bmp');
A = imread(strcat('J:\A2-
R2\',a(1).name));
A = rgb2gray(A);
A = A(178:728,208:681);
figure(1),imshow(A);
A = double(A);

for i = 2:100;
    B =
imread(strcat('J:\A2R2\',a(i).name));
    B = rgb2gray(B);
    B = B(178:728,208:681);
    B = double(B);
    A = A+B;
end
A = A/100;
A = uint8(A);
figure(2),imshow(A);

B = imread(strcat('J:\A2-
R2\',a(1).name));
B = rgb2gray(B);
B = B(178:728,208:681);
figure(3),imshow(B);
% B = B-A;%subtracting the background
image
figure(4),imshow(B);

b = imopen(B,strel('ball',4,2));
h = fspecial('motion',4,2);
b = imfilter(b,h,'conv','same');
B = B-b;
h = fspecial('unsharp');
H = imfilter(B,h);
h = fspecial('gaussian',4,0.95);
H = imfilter(H,h);
figure(5),imshow(H);

for i = 1:336;%Thresholding
    for j= 2:474;
    if   H(i+1,j-1)-H(i,j)<30;
         H(i,j)=0;
     end
     if   H(i+1,j-1)-H(i,j)>30;
         H(i,j)=255;
     end
    end
end
for i = 336:550;%Thresholding
    for j= 2:474;
    if   H(i,j)<25;
         H(i,j)=0;
     end
     if   H(i,j)>25;
         H(i,j)=255;
     end
    end
end
figure(6),imshow(H);
h = fspecial('gaussian',4,.95);
H = imfilter(H,h);
figure(7),imshow(H);
I = imfill(H,'holes');
I = imclearborder(I);
figure(8),imshow(I);
I = im2bw(I);
I = bwareaopen(I,4);%removing sizes
smaller than 4 pixels area
figure(9),imshow(I);

CC = bwconncomp(I);
L = labelmatrix(CC);
% RGB = label2rgb(L);
% figure(10), imshow(RGB)

% [L,N] = bwlabel(I);
D = regionprops(L,'All');
n = length(D);
W = [D.MajorAxisLength];
Wss = 14.2785*W;
figure(11),hist(Wss,100);
h = findobj(gca,'Type','patch');
set(h,'FaceColor','g','EdgeColor','k'
)
xlabel('Size/microns','Fontsize',12);
ylabel('number of
crystals','Fontsize',12);

Z = [D.MajorAxisLength];
Z1 = [D.MinorAxisLength];
Wss1 = 19*Z1;
for j = 1:length(D);
    e = 1-(Z1(:,j))/(W(:,j))
%Elongation
    N (j) = sum(e(:));
end
figure(12),hist(N,50);
h = findobj(gca,'Type','patch');
set(h,'FaceColor','g','EdgeColor','k'
)
figure(3),[n201, xout201] =
hist(D,98.5);
```

```
bar(xout201,n201/83,'g');hold
[n202, xout202] = hist(E,85);
bar(xout202,n202/50,'c');
[n203, xout203] = hist(F,94);
```

CSDs for 10 images of τ = 10, 20 and 30 minutes

```
clear all
close all
clc
 % 10mins
A =
xlsread('C:Name.xlsx','10mins','A1:A985')
;
B =
xlsread('C:Name.xlsx'.xlsx','10mins','B37
7:B5023');
C =
xlsread('Name.xlsx'.xlsx','10mins','C449:
C3199');
figure(1),hist(A,148);hold
h = findobj(gca,'Type','patch');
set(h,'FaceColor','c','EdgeColor','k');
hist(B,158,'c');
h = findobj(gca,'Type','patch');
set(h,'FaceColor','r','EdgeColor','k');
hist(C,103);
h = findobj(gca,'Type','patch');
set(h,'FaceColor','g','EdgeColor','k');

figure(2),[n1, xout1] = hist(A,74);
bar(xout1,n1/91,'g');hold
[n2, xout2] = hist(B,79);
bar(xout2,n2/40,'b');
[n3, xout3] = hist(C,52);
bar(xout3,n3/36,'r');
h = findobj(gca,'Type','patch');
xlabel('Size(µm)','Fontsize',12);
ylabel('number of
crystals(#/cm^3.µm)','Fontsize',12);
l =legend('10min1','10min2','10min3');
set(l,'Location','Best');
% 20 minutes
D =
xlsread('C:Name.xlsx','20mins','CK3:CK573
9');
E =xlsread('C:Name
.xlsx','20mins','CL5:CL3491');
F = xlsread('C:Name
xlabel('Size(µm)','Fontsize',12);
ylabel('number of
crystals(#/cm^3.µm)','Fontsize',12);
l =legend('10min','20min','30min');
set(l,'Location','Best');
versus time (Autosaved)1
(Autosaved).xlsx','20mins','CN3:CN9224');
G2 = xlsread('C:\Name
```

```
Nduna\Documents\Salt and Ice CSD
versus time (Autosaved)1
(Autosaved).xlsx','30mins','AA230:AA1
1690');
figure(4),[n10, xout10] =
hist(A1,94);
bar(xout10,n10/83,'g');hold
[n20, xout20] = hist(D1,90);
bar(xout20,n20/196,'b');
[n30, xout30] = hist(G2,53);
bar(xout30,n30/182,'r');
h = findobj(gca,'Type','patch');

bar(xout203,n203/28,'b');
l
=legend('20min1','20min2','20min3');
h = findobj(gca,'Type','patch');
xlabel('Size(µm)','Fontsize',12);
ylabel('number of
crystals(#/cm^3.µm)','Fontsize',12);
title('Ice CSD at 20 mins for
eutectic feed composition');

% 30mins
G =
xlsread('C:Name.xlsx','30mins','X85:X
4383');
H =
xlsread('C:Name.xlsx','30mins).xlsx',
'30mins','Y80:Y3877');
I =
xlsread('C:\Name.xlsx','30mins','Z71:
Z3434');
figure(3),[n30, xout30] = hist(G,92);
bar(xout30,n30/32,'g');hold
[n31, xout31] = hist(H,105);
bar(xout31,n31/31.8,'c');
[n32, xout32] = hist(I,93.6);
bar(xout32,n32/28,'b');
h = findobj(gca,'Type','patch');
xlabel('Size(µm)','Fontsize',12);
ylabel('number of
crystals(#/cm^3.µm)','Fontsize',12);
title('Ice CSD at 30 mins for 5wt%
feed composition');
```

9.2 Appendix 2

Ice CSD Analysis Algorithm

```
clc
clear all
close all
a = dir('C:\Name\*.bmp');
A =
imread(strcat('C:\Name\*.bmp\',a(1).name));
A = rgb2gray(A);
A = A(135:580,93:597);
figure(1),imshow(A);
A = double(A);
for i = 2:65;
C =
imread(strcat('C:\Name\*.bmp\',a(i).name));
       C = rgb2gray(C);
       C = C(135:580,93:597);
       C = double(C);
       A = A+C;
end
A = A/65;
A = uint8(A);
figure(2),imshow(A);

B =
imread(strcat('C:\Name\*.bmp',a(22).name));
B = B(135:580,93:597,:);
Badj1 = imadjust(B(:,:,1));
Badj2 = imadjust(B(:,:,2));
Badj3 = imadjust(B(:,:,3));

Ba(:,:,1) = Badj1;
Ba(:,:,2) = Badj2;
Ba(:,:,3) = Badj3;
Babw = rgb2gray(Ba);
figure(5),imshow(Babw);
% C = rgb2gray(C);
% C = C(135:580,93:597);
% % C =C(180:337,459:598);
% figure(3),imshow(C);
C = Babw-A;%subtracting the background
image
% figure(4),imshow(C);
b =
imopen(C,strel('ball',10,4));%background
with intensity
% correction for image
figure(6),imshow(b);
% H = fspecial('gaussian',10,11);
% b = imfilter(b,H,'replicate');
% C = C-b;
figure(60),imshow(C);
% h = fspecial('unsharp');
% H = imfilter(C,h);
% figure(5),imshow(H)

h = findobj(gca,'Type','patch');

crystals','Fontsize',12);
set(h,'FaceColor','g','EdgeColor','k')
xlabel('Elongation','Fontsize',12);
ylabel('number of
crystals','Fontsize',12);
title('Salt elongation at 20 mins for
a eutectic feed composition');
h = fspecial('gaussian',4,0.8);
H = imfilter(C,h);
figure(6),imshow(H);

for j = 1:446;
    for k=1:505;
     if   H(j,k)<40;
          H(j,k)=0;
     end
    if   H(j,k)>40;
          H(j,k)=255;
     end
    end
end
figure(8),imshow(H);
H = im2bw(H);
I = imfill(H,'holes');
H = bwareaopen(I,5);
figure(9),imshow(H);

C =imclearborder(C);
CC = bwconncomp(H);
L = labelmatrix(CC);
% RGB = label2rgb(L);
% figure(10), imshow(RGB);

% [L,N] = bwlabel(CC);
D =
regionprops(L,'Area','Eccentricity');
% n = length(D)
% n1 = size(D);

%Sodium sulphate decahydrate product
properties
e =
find([D.Eccentricity]>0.75&[D.Area]<15
0);
Lss = ismember(L,e);
figure(11),imshow(Lss);
S = regionprops(Lss,'All');
Wss = [S.MajorAxisLength];
Wss = 28.85*Wss;
Xav = mean(Wss);
std = std(Wss);
figure(12),hist(Wss,50);
h = findobj(gca,'Type','patch');
set(h,'FaceColor','g','EdgeColor','k')
xlabel('Size/microns','Fontsize',12);
ylabel('number of
%  B = B-A;
% H = fspecial('motion',30,60);
```

```
title('Salt CSD at 20 mins for eutectic
feed composition');

Z = [S.MajorAxisLength];
Z1= [S.MinorAxisLength];
for j = 1:length(S);
    e = 1-(Z1(:,j))/(Z(:,j)); %Elongation
    N(j) = sum(e(:));
end
figure(13),hist(N,20);
figure(20),imshow(B);
%Ice product characteristics
e1 =
find([D.Eccentricity]<=0.75|[D.Area]>=200);
Lice = ismember(L,e1);
figure(14),imshow(Lice);

Sice = regionprops(Lice,'All');
Wice = [Sice.Area];
Wice = 19.9*sqrt(4*Wice/pi);
X10_ice = mean(Wice);
% std = std(Wice);
figure(15),hist(Wice,200);
h = findobj(gca,'Type','patch');
set(h,'FaceColor','g','EdgeColor','k');
xlabel('Size/microns','Fontsize',12);
ylabel('number of crystals','Fontsize',12);
title('Ice CSD at 20 mins for eutectic feed
composition');
```

Thresholding using edge detection

```
clc
clear all
close all

a = dir('C:\Users\Moses
Nduna\Desktop\10rpm1\*.bmp');
A = imread(strcat('C:\Users\Moses
Nduna\Desktop\10rpm1\',a(1).name));
A = rgb2gray(A);
A = A(190:418,112:600);
figure(1),imshow(A);
A = double(A);
for i = 1:65;
    C = imread(strcat('C:\Users\Moses
Nduna\Desktop\10rpm1\',a(i).name));
       C = rgb2gray(C);
       C = double(C);
       C = C(190:418,112:600);
       A = A+C;
end
A = A/65;
A = uint8(A);
figure(2),imshow(A);
B = imread(strcat('C:\Users\Moses
Nduna\Desktop\10rpm1\',a(61).name));
B = rgb2gray(B);
B = B(190:418,112:600);
%       end
%     if   B(i,j)>100;
% b = imfilter(b1,H,'replicate');
% B = (B1+B)/2;
% B = imadjust(B);
I = imfill(B,'holes');
% H = bwareaopen(I,4);
% figure(10),imshow(H);
h = fspecial('gaussian',4,3);
% H = imfilter(B,h);
% figure(7),imshow(H);
E = edge(B,'canny',0.00000009,1.5)+
edge(B,'zerocross',0.00000000000009);
figure(40),imshow(E);
I = imfill(E,'holes');
figure(200),imshow(I);
%  for i = 1:184;
%     for j =1:237;
%      if  B(i,j)<40;
%          B(i,j)=0;
%      end
%     if   B(i,j)>=40;
%          B(i,j)=255;
%      end
%     end
%  end
%     for i = 1:184;
%     for j = 237:501;
%      if  B(i,j)<50;
%          B(i,j)=0;
%      end
%     if   B(i,j)>=50;
%          B(i,j)=255;
%      end
%     end
%     end
% for i = 184:409;
%     for j =1:221;
%      if  B(i,j)<80;
%          B(i,j)=0;
%      end
%     if   B(i,j)>80;
%          B(i,j)=255;
%      end
%     end
% end
%   for i = 184:409;
%     for j = 221:502;
%      if  B(i,j)<80;
%          B(i,j)=0;
%      end
%     if   B(i,j)>80;
%          B(i,j)=255;
%      end
%     end
%     end
%
%     for i = 1:420;
%     for j = 1:501;
%      if  B(i,j)<100;
%          B(i,j)=0;
legend('20mins1','20mins2','20mins3','
20mins1','20mins2','20mins3');
```

```
%           B(i,j)=255;
%       end
%     end
%     end
H =imclearborder(E);
CC = bwconncomp(H);
L = labelmatrix(CC);
% RGB = label2rgb(L);
% figure(10), imshow(RGB);
% [L,N] = bwlabel(CC);
D = regionprops(L,'All');
% n = length(D)
% n1 = size(D);

%Sodium sulphate decahydrate product
properties
e =
find([D.Eccentricity]>0.5&[D.MinorAxisLengt
h]<8);
Lss = ismember(L,e);
figure(11),imshow(Lss);
S = regionprops(Lss,'All');
Wss = [S.MajorAxisLength];
Wss = 19*Wss;%28.85 original

figure(12),hist(Wss,50);
h = findobj(gca,'Type','patch');
set(h,'FaceColor','g','EdgeColor','k')
xlabel('Size/microns','Fontsize',12);
ylabel('number of crystals','Fontsize',12);
title('Salt CSD at 20 mins for eutectic
feed composition');

Z = [S.MajorAxisLength];
Z1= [S.MinorAxisLength];
for j = 1:length(S);
    e = 1-(Z1(:,j))/(Z(:,j)); %Elongation
    N(j) = sum(e(:));
end
figure(13),hist(N,20);
h = findobj(gca,'Type','patch');
set(h,'FaceColor','g','EdgeColor','k')
xlabel('Elongation','Fontsize',12);
ylabel('number of crystals','Fontsize',12);
title('Salt elongation at 20 mins for a
eutectic feed composition');

%Ice product characteristics
e1 =
find([D.Eccentricity]<=0.5|[D.MinorAxisLeng
th]>=8);
Lice = ismember(L,e1);
figure(14),imshow(Lice);

hold on
figure(2),plot(Size,[a1*pdf201;a2*pdf202;a3
*pdf203]);
l =
% %30 minutes
D =
set(l,'Location','Best');
h = findobj(gca,'Type','patch');
xlabel('Size(µm)','Fontsize',12);
ylabel('number of
crystals(#/cm^3.µm)','Fontsize',12);

xlabel('Size/microns','Fontsize',12);
ylabel('number of
crystals','Fontsize',12);
title('Ice CSD at 20 mins for eutectic
feed composition');
I1 = B;
I1(Lice ==1|Lss) = 255;
figure(100),imshow(I1);

Sice = regionprops(Lice,'All');
Wice = [Sice.EquivDiameter];
Wice = 19*Wice;%28.85 og
X10_ice = mean(Wice);
% std = std(Wice);
figure(15),hist(Wice,100);
h = findobj(gca,'Type','patch');
set(h,'FaceColor','g','EdgeColor','k')
;
```

CSDs for Three Residence Times

```
clear all
close all
clc
%20 minutes
A = xlsread('C:\Users\Moses
Nduna\Documents\MatlabExcel
(Auto1).xlsx','3.7wt20mins','AN4:AN125
3');
B = xlsread('C:\Users\Moses
Nduna\Documents\MatlabExcel
(Auto1).xlsx','3.7wt20mins','AO4:AO151
9');
C = xlsread('C:\Users\Moses
Nduna\Documents\MatlabExcel
(Auto1).xlsx','3.7wt20mins','AP4:AP814
');
figure(1),[n201, xout201] =
hist(A,102);
bar(xout201,n201/19.4,'g');hold
[n202, xout202] = hist(B,120);
bar(xout202,n202/17,'b');
[n203, xout203] = hist(C,94.4);
bar(xout203,n203/12,'r');
h = findobj(gca,'Type','patch');
xlabel('Size(µm)','Fontsize',12);
ylabel('number of
crystals(#/cm^3.µm)','Fontsize',12);
l =legend('20min1','20min2','20min3');
set(l,'Location','Best');
% title('Ice CSD at 20 mins for
eutectic feed composition');

feed composition');
% bar(xout452,n452/26.3,'c');
```

```
xlsread('C:\Users\MosesNduna\Documents\Matl
abExcel
(Auto1).xlsx','3.7wt30mins','AZ5:AZ2254');
E = xlsread('C:\Users\Moses
Nduna\Documents\MatlabExcel
(Auto1).xlsx','3.7wt30mins','BA4:BA1160');
F = xlsread('C:\Users\Moses
Nduna\Documents\MatlabExcel
(Auto1).xlsx','3.7wt30mins','BB4:BB961');

figure(3),[n1, xout1] = hist(D,56);
bar(xout1,n1/20,'b');hold
[n2, xout2] = hist(E,93.8);
bar(xout2,n2/19.89,'r');
[n3, xout3] = hist(F,115);
bar(xout3,n3/12,'g');
h = findobj(gca,'Type','patch');
xlabel('Size(µm)','Fontsize',12);
ylabel('number of
crystals(#/cm^3.µm)','Fontsize',12);
l =legend('30min1','30min2','30min3');
set(l,'Location','Best');
title('Ice CSD at 30 mins for eutectic feed
composition');

% %45 minutes
% G = xlsread('C:\Users\Moses
Nduna\Documents\MatlabExcel
(Auto1).xlsx','3.7wt45mins','DL4:DL1952');
% H =
xlsread('C:\Users\MosesNduna\Documents\Matl
abExcel(Auto1).xlsx','3.7wt45mins','DM4:DM1
408');
% I = xlsread('C:\Users\Moses
Nduna\Documents\MatlabExcel(Auto1).xlsx','3
.7wt45mins','DN4:DN691');

figure(1),[n1, xout1] = hist(A,160);
bar(xout1,n1/75.4,'g');hold
[n2, xout2] = hist(B,168);
bar(xout2,n2/70.9,'r');
[n3, xout3] = hist(C,63.8);
bar(xout3,n3/26.63,'b');
h = findobj(gca,'Type','patch');
xlabel('Size(µm)','Fontsize',12);
ylabel('number of
crystals(#/cm^3.µm','Fontsize',12);

Size = linspace(43,1000);
pdf201 = pdf(a,Size);
pdf202 = pdf(b,Size);
pdf203 =pdf(e,Size);

% h = findobj(gca,'Type','patch');
% xlabel('Size(µm)','Fontsize',12);
% ylabel('number of
crystals(#/cm^3.µm)','Fontsize',12);
% title('Ice CSD at 45 mins for eutectic
```

```
% [n453, xout453] = hist(I,155);
% bar(xout453,n453/9.6,'b');

title('Ice CSD at 45 mins for eutectic
feed composition and 0.1 °C');

a1 =sum(n201/19.4)*(xout201(2)-
xout201(1));
a2 =sum(n202/17)*(xout202(2)-
xout202(1));
a3 =sum(n203/12)*(xout203(2)-
xout203(1));

% figure(4),[n451, xout451] =
hist(G,160);
% bar(xout451,n451/21.4,'g');hold
% [n452, xout452] = hist(H,124);
bar(xout15,n15/46.8,'g');hold
[n25, xout25] = hist(B,82);
bar(xout25,n25/39.1,'r');
[n35, xout35] = hist(C,83);
bar(xout35,n35/24,'b');
h = findobj(gca,'Type','patch');
xlabel('Size(µm)','Fontsize',12);
ylabel('number of
crystals(#/cm^3.µm','Fontsize',12);
title('Ice CSD at 30 mins for eutectic
feed composition and 0.1 oC');
```

Particle sizes at different temperatures

```
close all
clear all
clc

%T =-1.2°C at 30mins
A = xlsread('C:\Users\Moses
Nduna\Documents\Matlabsup.xlsx','Sup01
','C4:C1649');
B = xlsread('C:\Users\Moses
Nduna\Documents\Matlabsup.xlsx','Sup01
','D4:D822');
C = xlsread('C:\Users\Moses
Nduna\Documents\Matlabsup.xlsx','Sup01
','E4:E1766');
T =-1.11 at 30mins
G = xlsread('C C:Name
.xlsx','3.7wt30mins','AZ5:AZ2254');
H = xlsread( C:Name
.xlsx','3.7wt30mins','BA4:BA1160');
I = xlsread( C:Name
.xlsx','3.7wt30mins','BB4:BB961');
figure(3),[n101, xout101] =
hist(G,56);
bar(xout101,n101/20,'b');hold
[n201, xout201] = hist(H,93.8);
bar(xout201,n201/19.89,'r');
[n301, xout301] = hist(I,115);
```

```
% T =-1.15°C at 30mins
D = xlsread('C:\Users\Moses
Nduna\Documents\Matlabsup.xlsx','Sup005','B
2:B1544');
E = xlsread('C:\Users\Moses
Nduna\Documents\Matlabsup.xlsx','Sup005','C
2:C1457');
F = xlsread('C:\Users\Moses
Nduna\Documents\Matlabsup.xlsx','Sup005','D
2:D1052');
figure(2),[n15, xout15] = hist(D,157);


%three temperatures
A1 = xlsread('C:\Users\Moses
Nduna\Documents\Matlabsup.xlsx','Sup01','F4
:F4231');
D1 = xlsread('C:\Users\Moses
Nduna\Documents\Matlabsup.xlsx','Sup005','E
2:E4051');
G1 =
xlsread('C:Name.xlsx','3.7wt30mins','BC4:BC
4294');
figure(10),[n111, xout111] = hist(A1,84);
bar(xout111,n111/348,'g');hold
[n211, xout211] = hist(D1,79);
bar(xout211,n211/221.6,'r');
[n311, xout311] = hist(G1,58);
bar(xout311,n311/104,'b');
h = findobj(gca,'Type','patch');
xlabel('Size(µm)','Fontsize',12);
ylabel('number of particles(#
/cm^3.µm)','Fontsize',12);
l =legend('T = -1.20°C','T = -1.15°C','T =
-1.11°C');
title('Ice CSD at supercoolings of 0.1,0.05
and 0.01°C at 30 mins residence time for
eutectic feed composition');
```

9.3 Appendix 3

Analysis of results for different supercoolings

```
clc
close all
clear all
a = dir('C:\Users\Moses
Nduna\Documents\c\*.bmp');
A = imread(strcat('C:\Users\Moses
Nduna\Documents\c\',a(1).name));
A = rgb2gray(A);
A = A(206:908,336:748);
figure(1),imshow(A);
A = double(A);

for i = 2:86;
    B = imread(strcat('C:\Users\Moses
Nduna\Documents\c\',a(i).name));
    B = rgb2gray(B);
    B = B(206:908,336:748);
    B = double(B);
    A = A+B;
end
A = A/100;
A = uint8(A);
figure(2),imshow(A)
B = imread(strcat('C:\Users\Moses
Nduna\Documents\c\',a(50).name));
B = B(80:796,530:860,:);
figure(3),imshow(B);

Badj1 = imadjust(B(:,:,1));
Badj2 = imadjust(B(:,:,2));
Badj3 = imadjust(B(:,:,3));

Ba(:,:,1) = Badj1;
Ba(:,:,2) = Badj2;
Ba(:,:,3) = Badj3;
Babw = rgb2gray(Ba);
figure(5),imshow(Babw);
 b = imopen(Babw,strel('disk',10));
h = fspecial('motion',10,30);
b = imfilter(b,h,'circ','conv');
Ba = Babw-b;
% Ba = imadjust(Ba);
figure(6),imshow(Ba);

h = fspecial('gaussian',4,0.8);
B = imfilter(Ba,h,'same');
figure(7),imshow(B);
for j = 1:717;
    for k=1:331;
     if  B(j,k)<12;
         B(j,k)=0;
     end

Dss = regionprops(Lss,'All');
% Wss = [Dss.MajorAxisLength];
% Wss = 19*Wss;
% Xav = mean(Wss);
if  B(j,k)>12;
         B(j,k)=255;
     end
    end
end
% for j = 261:561;
%     for k = 1:369;
%      if  B(j,k)<12;
%          B(j,k)=0;
%      end
%
%      if  B(j,k)>12;
%          B(j,k)=255;
%      end
%     end
% end
% for j = 562:819;
%     for k=1:220;
%      if  B(j,k)<38;
%          B(j,k)=0;
%      end
%
%      if  B(j,k)>38;
%          B(j,k)=255;
%      end
%     end
% end
%
% for j =562:819;
%     for k=221:369;
%      if  B(j,k)<12;
%          B(j,k)=0;
%      end
%
%      if  B(j,k)>12;
%          B(j,k)=255;
%      end
%     end
% end
figure(8),imshow(B);
H = imfill(B,'holes');
H =imclearborder(H);
H = bwareaopen(H,4);

CC = bwconncomp(H);
L = labelmatrix(CC);
% RGB = label2rgb(L);
% figure(10), imshow(RGB)

% [L,N] = bwlabel(I);
D = regionprops(L,'All');
% e =
find([D.Eccentricity]>=0.85&[D.Area]<
100);
% Lss = ismember(L,e);
% % Lss =bwareaopen(Lss);
% figure(10),imshow(Lss);
```

```
% figure(11),hist(Wss,50);
% h = findobj(gca,'Type','patch');
% set(h,'FaceColor','g','EdgeColor','k')
% xlabel('Size/microns','Fontsize',12);
% ylabel('number of
crystals/cm2','Fontsize',12);
% title('Sodium sulphate decahydrate CSD
for a eutectic feed compositionat 20
minutes');
%
% Z = [Dss.MajorAxisLength];
% Z1= [Dss.MinorAxisLength];
% for j = 1:length(Dss);
%     e(j) = 1 -(Z1(:,j))/(Z(:,j));
%     N(j) = sum(e(j));
% end
% figure(12),hist(N,20);
% h = findobj(gca,'Type','patch');
% set(h,'FaceColor','g','EdgeColor','k')
% xlabel('Elongation/[-]','Fontsize',12);
% ylabel('number of
crystals/cm2','Fontsize',12);
% title('Elongation distribution at 20
mins from an EFC image');

e1 =
find([D.Eccentricity]<0.5|[D.Area]>=100);
Lice =ismember(L,e1);
figure(13),imshow(Lice);

D2 = regionprops(Lice,'All');
Wice = [D2.EquivDiameter];
Wice = 23.8*Wice;
figure(14),hist(Wice,100);
h = findobj(gca,'Type','patch');
set(h,'FaceColor','g','EdgeColor','k')
xlabel('Size/microns','Fontsize',12);
ylabel('number of
crystals/cm2','Fontsize',12);
title('Ice crystal size distribution for
a eutectic feed composition at 20
minutes');

E = [D2.Eccentricity];
figure(15),hist(E,20);
h = findobj(gca,'Type','patch');
set(h,'FaceColor','g','EdgeColor',
'k');
xlabel('Eccentricity/[]');
ylabel('number of crystals');
title('Ice eccentricity distribution
for a eutectic feed compositionat at
20 mins residence time');
```

9.4 Appendix 4

Example of classified particle sizes for 30 minutes residence time

30 minutes Run2								
ΔL =							**10**	**µm**
L_{mid}(µm)	**n(#)**	**n(#/cm^3)**	**n' (#/cm^3.µm)**	**n(L_{mid}).L_{mid}**	**%n(L_{mid})**	**%n(<L_{mid})**	**N(#/m^3.µm)**	**lnN**
48	71	36	4	171	7	7	3569471	15
58	92	46	5	268	8	8	4625230	15
68	95	48	5	324	9	17	4776053	15
78	95	48	5	372	9	26	4776053	15
88	90	45	5	398	8	34	4524682	15
98	86	43	4	423	8	42	4323585	15
108	75	38	4	407	7	49	3770568	15
118	33	17	2	196	3	52	1659050	14
128	66	33	3	424	6	58	3318100	15
138	29	15	1	201	3	61	1457953	14
148	45	23	2	335	4	65	2262341	15
158	34	17	2	270	3	68	1709324	14
168	26	13	1	220	2	71	1307130	14
178	40	20	2	358	4	74	2010970	15
188	16	8	1	151	1	76	804388	14
198	24	12	1	239	2	78	1206582	14
208	18	9	1	188	2	80	904936	14
218	14	7	1	153	1	81	703839	13
228	12	6	1	138	1	82	603291	13
238	14	7	1	167	1	83	703839	13
248	13	7	1	162	1	84	653565	13
258	12	6	1	156	1	86	603291	13
268	12	6	1	162	1	87	603291	13
278	6	3	0	84	1	87	301645	13
288	14	7	1	203	1	88	703839	13
298	12	6	1	180	1	90	603291	13
308	14	7	1	217	1	91	703839	13
318	4	2	0	64	0	91	201097	12
328	7	4	0	115	1	92	351920	13
338	13	7	1	221	1	93	653565	13
348	4	2	0	70	0	93	201097	12
358	8	4	0	144	1	94	402194	13
368	4	2	0	74	0	95	201097	12
378	5	3	0	95	0	95	251371	12
388	3	2	0	59	0	95	150823	12
398	5	3	0	100	0	96	251371	12
408	1	1	0	21	0	96	50274	11

418	4	2	0	84	0	96	201097	12
428	1	1	0	22	0	96	50274	11
438	3	2	0	66	0	97	150823	12
448	3	2	0	68	0	97	150823	12
458	3	2	0	69	0	97	150823	12
468	1	1	0	24	0	97	50274	11
478	2	1	0	48	0	97	100548	12
488	1	1	0	25	0	98	50274	11
498	6	3	0	150	1	98	301645	13
508	3	2	0	77	0	98	150823	12
518	2	1	0	52	0	99	100548	12
528	1	1	0	27	0	99	50274	11
538	1	1	0	27	0	99	50274	11
558	2	1	0	56	0	99	100548	12
568	4	2	0	114	0	99	201097	12
578	1	1	0	29	0	99	50274	11
658	1	1	0	33	0	99	50274	11
678	1	1	0	34	0	100	50274	11
758	1	1	0	38	0	100	50274	11
848	1	1	0	43	0	100	50274	11
858	1	1	0	43	0	100	50274	11
948	1	1	0	48	0	100	50274	11
968	1	1	0	49	0	100	50274	11
Total		**582**	**55**	**8580**	**100**	**4928**		
Mean(µm)								**157**

9.5 Appendix 5

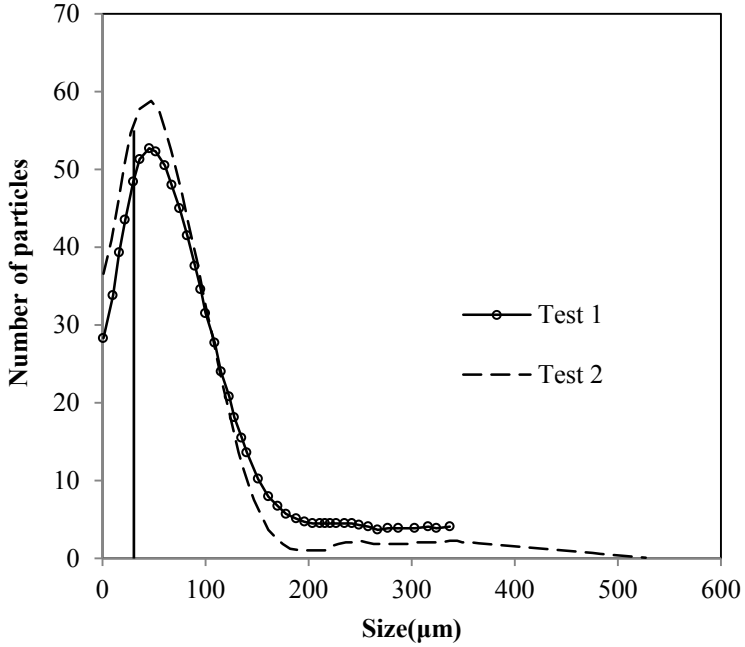

Figure 9.1 : Crystal size distribution of $Na_2SO_4.10H_2O$ measured using an optical microscope

Particle sizes below 30 µm (to the left of vertical line) could not be measured using a digital camera and this constituted close to 20 % of the particle population. However, this comprised less than 1% of the total mass of the solid phase as estimated from the third moment of the size distribution.

$$w_T(L < 30) = \frac{\sum_0^{29} k_v \rho n(L) L^3 \Delta L}{\sum_0^{600} k_v \rho N(L) L^3 \Delta L}$$

Assuming similar crystal density, ρ_c and shape factor, k_v the weight fraction of particles with sizes less than 30 µm was estimated to be 0.04 and 0.05 % for Test 1 and Test 2 respectively.

$$w_T = \frac{5^3 \times 62 + 15^3 \times 34 + 25^3 \times 44}{5^3 \times 62 + 15^3 \times 34 + 25^3 \times 44 + \cdots . + 335^3 \times 4} \times 100$$

$$= 0.04\ \%$$

The mass of particles was therefore assumed to be negligible compared to the total mass although the relative abundance was quite significant.